

Characterization of Cyclic and Linear Dipeptides

A Thesis

Presented to

The Faculty of the Department of Chemistry

The College of William & Mary in Virginia

In Partial Fulfillment

Of the Requirements for the Degree of

Master of Arts

by

Christine Michelle Howard

2001

Approval Sheet

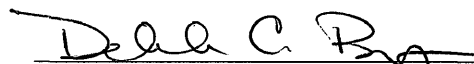
This thesis is submitted in partial fulfillment

Of the requirements for the degree of

Master of Arts


Author

Approved, September 2001


Deborah C. Bebout


Christopher J. Abelt

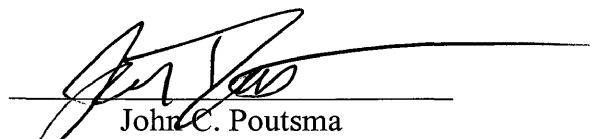

John C. Poutsma

TABLE OF CONTENTS

	Page
ACKNOWLEDGMENTS	iv
LIST OF FIGURES	v
ABSTRACT	vii
INTRODUCTION	2
EXPERIMENTAL	18
RESULTS AND DISCUSSIONS	
I. Organic Syntheses	
Synthesis of cAH	30
Synthesis of cHH	31
Synthesis of cAM	32
Synthesis of cLP	34
II. Analysis of Cyclo(L-Leucyl-D-Prolyl) by Mass Spectrometry	36
III. Cyclo(L-Leucyl-D-Prolyl) Integration into β Cyclodextrin	38
IV. NMR Solution State Studies of Mercury (II) Coordination	
Solution State Investigations of cMM	39
Solution State Investigations of cAM	43
Solution State Investigations of cHH	47
Solution State Investigations of cAH	51
V. NMR Solution State Studies of Cadmium (II) Coordination	56
CONCLUSION	60

APPENDIX	62
REFERENCES	74
VITA	77

ACKNOWLEDGMENTS

I would like to thank Dr. Bebout for her never-ending patience, guidance and encouragement throughout the course of my research. I would like to thank Dr. Vold, Dr. Hoatson, and Dr. Poutsma for their willingness to undertake the study of dipeptides and assist me in my research. In addition, I would like to recognize the research performed by previous students Sagar Damle and Janice Jones, whose work provided the foundation of this study. I would like to thank the other members of the laboratory group and the other graduate students, both recently graduated and present, for their assistance and support over the last several years. I would like to especially thank each member of my defense committee for their support, encouragement, and assistance. Finally, I would like to thank Geoff and my family for all of their love and support, without which the completion of this project would not have been possible.

LIST OF FIGURES

Figure	Page
1. Simplistic model of protein folding	10
2. The metal induced cyclic dipeptide “folding” process.	11
3. Planar conformation of DOP ring	15
4. Flagpole boat conformation of DOP ring	15
5. Bowspirit boat conformation of DOP ring	15
6. Histidine	15
7. Methionine	15
8. Alanine	15
9. Cyclo(L-Methionyl-L-Methionyl)	16
10. Cyclo(L-Histidyl-L-Histidyl)	16
11. Cyclo(L-Alanyl-L-Methionyl)	16
12. Cyclo(L-Alanyl-L-Histidyl)	16
13. Cyclo(L-Leucyl-D-Prolyl)	17
14. Synthesis of Cyclo(L-Alanyl-L-Histidyl)	31
15. Synthesis of Cyclo(L-Histidyl-L-Histidyl)	32
16. Synthesis of Cyclo(L-Alanyl-L-Methionyl)	33
17. Synthesis of Cyclo(L-Leucyl-D-Prolyl)	35
18. Mass Spectrometric Fragmentation of cLP	37
19. cMM	39
20. The chemical shifts of protons of cMM as a function of the Hg(ClO ₄) ₂ to cMM ratio in DMSO-d ₆ at room temperature.	40

Figure	Page
21. Stack plot of selected NMR runs of cMM as a function of the Hg(ClO ₄) ₂ to cMM ratio in DMSO-d ₆ at room temperature.	41
22. The chemical shifts of protons of cAM as a function of the Hg(ClO ₄) ₂ to cAM ratio in DMSO-d ₆ at room temperature.	44
23. Stack plot of selected NMR runs of cAM as a function of the Hg(ClO ₄) ₂ to cAM ratio in DMSO-d ₆ at room temperature.	45
24. cAM	43
25. The chemical shifts of protons of cHH as a function of the Hg(ClO ₄) ₂ to cHH ratio in DMSO-d ₆ at 20°C.	48
26. Stack plot of selected NMR runs of cHH as a function of the Hg(ClO ₄) ₂ to cHH ratio in DMSO-d ₆ at 20°C.	49
27. cHH	47
28. The chemical shifts of protons of cAH as a function of the Hg(ClO ₄) ₂ to cAH ratio in DMSO-d ₆ at 20°C.	52
29. Stack plot of selected NMR runs of cAH as a function of the Hg(ClO ₄) ₂ to cAH ratio in DMSO-d ₆ at 20°C	53
30. cAH	54
31. The chemical shifts of protons of cHH as a function of the Cd(ClO ₄) ₂ ·H ₂ O to cHH ratio in DMSO-d ₆ at room temperature.	57
32. Stack plot of selected NMR runs of cHH as a function of the Cd(ClO ₄) ₂ ·H ₂ O to cHH ratio in DMSO-d ₆ at room temperature.	58

ABSTRACT

The mercury coordination chemistry of the cyclic dipeptides cyclo(L-alanyl-L-histidyl) (cAH), cyclo(L-histidyl-L-histidyl) (cHH), cyclo(L-alanyl-L-methionyl) (cAM), and cyclo(L-methionyl-L-methionyl) (cMM) was investigated by proton NMR. Comparisons were made between the studies of cyclo(L-histidyl-L-histidyl) and cyclo(L-alanyl-L-histidyl), as well as between the cyclo(L-methionyl-L-methionyl) and cyclo(L-alanyl-L-methionyl) studies. Trends in chemical shift as a function of the metal-to-dipeptide ratio were examined, and analysis of the Hg(II):cAM and Hg(II):cMM titration studies suggest the possibility of sulfur-mercury(II) interaction. The δ nitrogen of the histidyl side chain was tentatively established as the primary coordination site for Hg(II) from analysis of the titration studies of Hg(II):cAH and Hg(II):cHH. Cadmium(II):cHH titration studies suggest the possible formation of a 1:2 Cd(II):cHH complex. Also, cyclo(L-leucyl-D-prolyl) was synthesized for future solid state NMR evaluation of molecular motion in the pure form and as an inclusion complex of a cyclodextrin. Cyclo(L-leucyl-D-prolyl) was also fragmented using mass spectrometry and linear intermediates of this dipeptide were prepared for future analysis by mass spectrometry.

Characterization of Cyclic and Linear Dipeptides

INTRODUCTION

Imagining a cellular world without proteins is a very difficult, if not impossible, task. Enzyme catalysis dictates physiological conditions in every cell. Furthermore, proteins give cells structural support and regulate gene expression. Proteins transport energy during photosynthesis and provide defense against foreign invasion. Even more remarkable is that proteins can perform all these functions with different numbers and sequences of only 20 amino acids.

Over 30 years ago, Anfinsen and his colleagues proposed that the linear sequence of amino acids determines the final three-dimensional folded structure of a protein.¹ The three-dimensional shape of the native protein is what is required for proteins to achieve complete biological activity. Errors within the native protein structure or problems with the protein folding mechanisms within the cellular environment are the basis for numerous human diseases.² There are several types of interactions that help to properly stabilize the native structure of a protein so that proper folding occurs. These stabilizing elements include interactions between amino acids within the same protein chain and amino acids on different protein chains, as well as hydrophobic and hydrophilic interactions with the surrounding environment. Protein structure can also be stabilized by interactions between amino acid cofactors, like metal ions. While there have been many recent developments and advances in the characterization of proteins by mass spectrometry, X-ray diffraction, and multinuclear NMR techniques, our understanding of the folding process is still very limited.

Tandem mass spectrometry is a technique that can be used to determine a protein's fragmentation pattern, thereby predicting the strength of bonds within the compound. X-ray crystallography is a technique used to obtain detailed structural information about the metal binding sites of native proteins. Large, well-ordered crystals of the protein are vital to determination of protein structure by this technique. Solution-state NMR, on the other hand, does not require well-formed crystals, and enables the characterization of metal-ligand interactions in solution, through the study of nuclear shielding interactions between the electron clouds of the ligand and metal. Solid-state NMR provides an opportunity to monitor characteristics of disordered solids, and relate them to physical properties and molecular motion.

Mass Spectrometry

Mass spectrometry is an analytical technique in which analytes are converted to gas-phase ions, which are subsequently separated by their mass-to-charge ratio.³ The resulting display of ion abundance vs. mass-to-charge ratio is the mass spectrum of the analyte.³ Early mass spectrometers were based on the deflection of ions moving in a magnetic field.⁴ The sample was introduced, as a vapor, into a vacuum chamber where positive ions were formed by electron bombardment. Negatively charged plates at one end of the chamber then accelerated the parent ions and product ions resulting from subsequent fragmentation through the magnetic field.⁴ The degree of deflection in the magnetic field was based on the ion's mass, velocity, and charge, and the amount of deflection was inversely proportional to each fragment's mass. Ions of interest were

detected in an ion collector, where an electronic signal was generated and amplified prior to recording the results as a function of mass-to-charge ratio.⁴

This technique proved unsuitable for protein analysis primarily because proteins are non-volatile compounds and denature when heated. The recently developed techniques of electrospray ionization (ESI) and matrix-assisted laser desorption ionization (MALDI), however, have permitted researchers to analyze proteins and other large biomolecules.⁵ In an ESI experiment, the pH of a solution is varied to form ions in solution, which are transferred to the gas phase via electric potential.⁵ In contrast, MALDI experiments use lasers to ionize some organic matrix, in which the analytes of interest are dissolved.⁵ These two ion sources have allowed both single stage and tandem mass spectrometry experiments to be performed on biomolecules.

Tandem mass spectrometry (MS/MS) is a technique that was developed to analyze complex mixtures.³ MS/MS also provides researchers with the opportunity to elucidate the structures of large molecules, which is virtually impossible with single-stage mass spectrometry. MS/MS experiments can be performed with the two stages of mass spectrometry (MS-I and MS-II) separated either in space or in time. Separating the two stages of mass spectrometry in space involves the use of multiple mass analyzers, such as multiple quadrupoles or tandem sectors, which are physically separated. A soft ionization source, such as chemical ionization or ESI, is used to produce analyte molecular ions with little or no fragment ions. MS-I allows only ions of a particular mass-to-charge ratio to pass through its exit slit. The ions then enter a collision chamber, usually an rf-only quadrupole, where ions collide with an inert gas, such as argon or xenon, to induce further dissociation of the ion.³ This type of fragmentation is called

collision-induced dissociation (CID). The resulting product ions are then directed into MS-II.³ Since CID produces many characteristic product ions, the identity of the parent ion can usually be determined when these product ions are analyzed in the second mass spectrometer.

The second MS/MS method involves trapping ions in one place so that multiple stages of mass spectrometry can be performed sequentially in time. Ions accumulate in the ion trap and ions with a single mass-to-charge ratio (m/z) of interest are selected. All other m/z are removed from the ion trap. The mass-selected ion is then fragmented and the product ions are analyzed in a second stage of mass spectrometry in the same environment. Both tandem mass spectrometry techniques hold great promise in the future characterization of proteins, as they will provide confirmation of peptide sequence, as well as providing insight into bond strengths and weaknesses within proteins.

X-ray Crystallography

X-ray crystallography is a useful technique that can determine the detailed structure of a protein using a single, well-ordered crystal. Unfortunately, crystallization is impeded by the irregular surfaces of proteins. Furthermore, mechanism of metal ion incorporation into a protein cannot be determined by X-ray analysis. Nuclear magnetic resonance (NMR), however, allows for proteins to be studied in solution and as solids, providing a valuable complement to information obtained through X-ray crystallography and mass spectrometry.

Nuclear Magnetic Resonance

NMR is a useful technique for structural characterization because it is potentially applicable to all nuclei possessing nuclear spin. Isotopes with suitable spin qualities have an odd atomic weight or an odd number of protons and neutrons. A magnetic field is created by the spinning motion of charged nuclei. Nuclei with spin $I = \frac{1}{2}$ are favored in NMR experiments as there is a marked reduction in the quality of NMR information available for nuclei with spin $I > \frac{1}{2}$. Two possible spin states arise when the magnetic field of a spin $\frac{1}{2}$ nucleus interacts with a magnetic field of greater magnitude. The nuclear spin vector may be either aligned with the large magnetic field or against it. Alignment with the external magnetic field is more energetically favorable for the nucleus and a slight excess of nuclei populate the lower energy spin state in accordance with the Boltzmann distribution constant.⁶

NMR spectroscopy involves excitation between available spin states. Radiofrequency radiation can be used to excite the nuclear spin vector into a higher energy level(s), producing a non-equilibrated distribution of spin states. Free induction decay (FID), the result of vector relaxation back to equilibrium, produces a series of exponentially decaying sine waves, whose amplitudes are plotted as a function of frequency. A typical NMR is the result of a Fourier transformation of this data, and is particularly useful as not all nuclei of the same type resonate at the same frequency and field. A precession frequency of

$$\omega = \gamma(1 - \sigma)B_0$$

results from the phenomenon called shielding, where γ is equal to the magnetogyric ratio, a constant that describes how much magnetism arises from the spin and σ equals the

shielding parameter. This effect is called chemical shift and varies depending on the degree of shielding of a particular nucleus and the specific bonds involved.⁷

Spin coupling is an important aspect of NMR that provides information about the environment of a given nucleus.⁸ Coupling manifests itself in an NMR spectrum as a split peak. Coupling occurs when through-bond connectivity between two nuclei exists.⁷ Splitting arises because nuclear spins can be coupled via bonded electrons. The result is that the nuclei experience two different microenvironments and thereby each resonates at two slightly different frequencies. This frequency difference is equal to the scalar spin coupling constant J . The number of types of bonds through which the nuclei are coupled determines the magnitude of J . Further, the Karplus relationship

$$J_{xy} = A \cos 2\phi + B \cos \phi + C$$

where A , B , and C are empirical constants and ϕ is the dihedral angle, can be used in conjunction with coupling constants to determine dihedral bond angles.⁷ However, the relationship is a causal one, as two different angles can produce the same coupling constant.⁷

High-resolution NMR spectra of quadrupolar nuclei can be obtained from solid-state samples. MQ-MAS (multiple quantum magic-angle spinning) is a solid-state NMR technique that can be employed using conventional NMR spectrometers and probes. In general, solid-state NMR produces much broader, overlapping spectral lines than solution-state NMR. The low sensitivity of solid-state NMR also imposes the need to signal average multiple spectra to improve the poor signal-to-noise ratios.⁹ The lower signal-to-noise ratio of solid-state NMR compared to solution-state NMR can be attributed to the different NMR spectrum of each molecular orientation in a solid

compound, whereas with solution-state NMR these differences are averaged out by molecular tumbling. However, MAS can be utilized to overcome the drawbacks of spectral broadening and low signal-to-noise ratios as it narrows spectral lines by emulating the molecular tumbling observed with solution-state NMR. Employing MAS involves spinning samples in a rotor with an axis of 54.74° with respect to the magnetic field. A cubically symmetrical motion, which is imposed by the trajectory, is an adequate approximation to spherically symmetric motion that spectral broadening is averaged away and relatively sharp NMR resonances are obtained.⁹

Metal Ion Coordination to Proteins

The ideal heteronuclear NMR probe possesses spin $I = \frac{1}{2}$ nuclei, which have narrow resonance ranges, thereby permitting the detection of heteronuclear coupling. Abundant nuclei associated with a wide chemical shift range and large coupling constants are most useful in NMR studies. Biologically relevant spin $I = \frac{1}{2}$ nuclei include ^1H , ^{13}C , ^{15}N , and ^{113}Cd . The natural abundance of these nuclei ranges from 1.1% (^{13}C) to 99.9% (^1H). The chemical shift ranges of these nuclei also vary. Proton NMR is frequently used to characterize proteins, unfortunately the limited chemical shift range of this nucleus leads to considerable spectral overlap. ^{13}C and ^{15}N are also somewhat unfavorable, as they are both of low natural abundance. Fortunately, many proteins incorporate metal ions into their active sites and NMR characterization of these metal-binding sites may provide valuable information. Unfortunately, none of the physiologically relevant metals (e.g. copper, zinc, iron and magnesium) have isotopes with favorable NMR properties. In

some cases, however, it is possible to substitute metals possessing favorable NMR properties for native metal ions and obtain relevant spectroscopic information.

$^{199}\text{Hg(II)}$ is one metal ion that possesses favorable NMR characteristics. This ion has a chemical shift range of more than 3000 parts per million.¹⁰ ^{199}Hg is the only spin $I = \frac{1}{2}$ isotope of mercury. It has a natural abundance of 16.8% and large coupling constants.¹⁰ In addition, it has a receptivity 5.4 times greater than ^{13}C and its chemical shift is very sensitive to the number and identity of bound nuclei.¹¹ Mercury NMR may thus prove to be a valuable technique for elucidating aspects of metalloprotein structure and folding.

Mercury is known to form complexes with nitrogen, sulfur and phosphorous with stability rarely exceeded by any other divalent cation. When compared to several physiologically essential transition elements, mercury exhibits similar charge and coordination geometry preferences. Metal binding studies have shown competition between mercury, zinc and copper for protein binding.¹² In several instances, metalloenzymes with mercury in place of the normal metal have retained catalytic activity.¹⁰ Several mercury-substituted proteins have been characterized by recently developed multinuclear NMR techniques demonstrating preservation of protein structure.¹³ However, an understanding of how and why proteins fold still eludes researchers.

Greater knowledge of protein folding processes will ultimately contribute to a better understanding of biological systems, as proteins are important in all of the metabolic pathways of living organisms. Studies of metal binding to peptides will also assist in the understanding of metal binding by proteins, which is important because

metal ion transport in body fluids and through membranes is strongly dependent on the relative complexing ability of amino acids and their peptides. A better understanding of the mechanism of protein folding itself may provide effective therapies for diseases caused by altered protein folding, such as Alzheimer's and scrapie.²

Three-dimensional folding of a polypeptide is, however, a very complex process. Proteins are synthesized by sequential addition of amino acids onto a linear chain. Since the folded structure brings amino acids far apart on the chain close together, the exposed end of the growing protein chain must remain at least partially unfolded until amino acid assembly is completed. Furthermore, proteins must fold in a heterogeneous aqueous solution, which provides numerous opportunities for folding/misassociation errors. Cells have evolved mechanisms, like molecular chaperones, which are responsible for preventing misassociations and facilitating proper folding under optimal cell conditions. In addition, some proteins require association with ions or small molecules to perform their catalytic function. There is some evidence that these cofactors may sometimes participate in the folding process.¹²

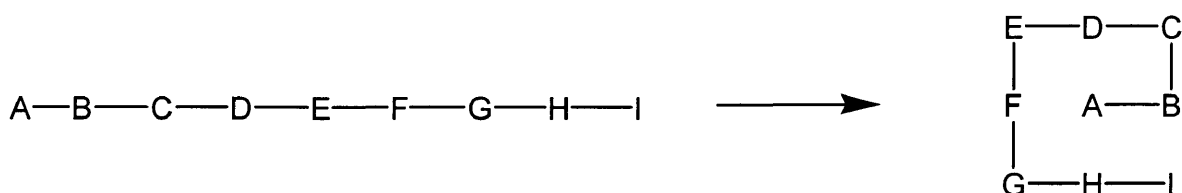


Figure 1: Simplistic model of protein folding.

Most protein folding studies have focused on the unimolecular process for proteins containing a single amino acid chain and no cofactors. Much simpler model studies are necessary to develop new tools for investigation of the more complex

bimolecular process involved in folding a metalloprotein. Through the detection of heteronuclear ^1H -metal coupling, previous protein metal binding site model studies have demonstrated Hg(II) binding in solution with both tridentate and tetradentate ligands, but not lower coordinate ligands. Both tetradentate and tridentate ligands have limited degrees of freedom and provide a claw-like feature in binding, thus the development of an even simpler protein model with similar features would be ideal for future protein folding studies.

Cyclic dipeptides possess a diketopiperazine ring system which restricts the degrees of freedom of metal coordinating amino acid side chains. When the diketopiperazine ring is in the "boat conformation", the amino acid side chains are oriented for pincher-like metal coordination. Cyclic dipeptides can thus be used to mimic

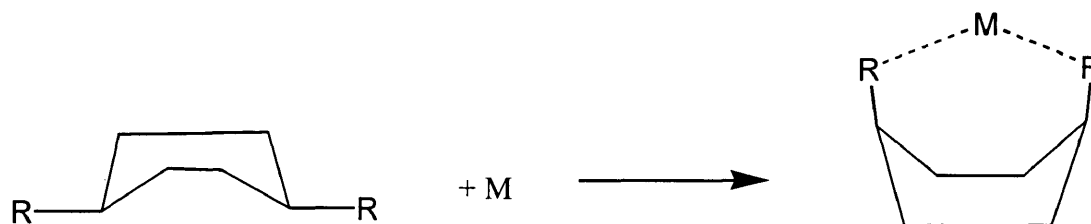


Figure 2: The metal induced cyclic dipeptide "folding" process. R is a metal binding group.

the close proximity of two amino acid side chains bound to a metal ion in a protein active site. Furthermore, cyclic dipeptides provide an alternative to studying entire proteins by reducing the high variability associated with linear peptide chains and by achieving

greater structural simplicity for characterization by X-ray diffraction, solution-state NMR studies, solid-state NMR studies, mass spectrometry*, and circular dichroism.

Many functional groups in proteins and peptides are potential metal coordination sites, as demonstrated in studies of metal binding with simple amino acids and other compounds. Histidine, for example, is a substantial contributors to protein structure and function and an essential amino acids in infants.¹⁴ Histidine residues bind heme prosthetic groups in hemoglobin.¹⁴ Methionine is another biologically important residue often encountered in the metal binding sites of proteins. Methionine is also an appropriate component for metal-bound ligands in mercury coordination studies because mercury forms a stable Hg-S bond to sulfur containing amino acid residues, resulting in “tight binding” to proteins in living systems.¹⁵ Investigating methionine and histidine interactions with mercury (II) will thus provide valuable insight that will aid in further understanding protein-metal interactions.

Past Studies

Metal Ion/Amino Acid Interactions

To date, there are few detailed studies of metal ion interactions, excluding terminal functional group effects, with side chain substituents and an amide linkage. In one existing study, four criteria were used to create model ligands for characterizing Cu(II) interactions with protein side chains and amide linkages.¹⁶ First, terminal carboxyl or amine groups were excluded from model ligands, except specifically as a side chain

* Uncoordinated cyclic dipeptides will be characterized with mass spectrometry, whereas both uncoordinated and metal-coordinated cyclic dipeptides will be studied by X-ray diffraction, solution-state NMR, solid-state NMR, and circular dichroism.

function. Second, model ligands were required to possess an amide linkage α to the substituted carbon of any amino acid residue. Third, the model ligands had to be easily prepared from a variety of natural and synthetic amino acids. Finally, the model ligands were kept sterically simple, but amenable to synthetic modification. These guidelines are applicable to cyclic dipeptides proposed for ^{199}Hg NMR studies.¹⁶

^{199}Hg NMR Studies of Mercury (II) Substituted Metalloproteins

The mercury ion has chemical characteristics suitable for ^{199}Hg and ^1H NMR investigation of the structure and function of biopolymers. Mercury (II) preserves catalytic activity when substituted for native metal ions of several metalloenzymes.¹⁵ Mercury also adopts the coordination environments of native metals as determined by a combination of ^{199}Hg NMR techniques, when substituted into a variety of Fe, Cu and Zn metalloproteins.¹⁷ ^{199}Hg NMR provided insight into allostery of MerR-DNA interactions.¹⁷ The MerR protein activates transcription of genes responsible for mercury detoxification after changes in intracellular metal ion concentration are detected. The conformation of MerR, and its biological activity as a transcription activator, are Hg(II) dependent.

Previous NMR and circular dichroism (CD) studies characterizing tetrapeptides have also been used to establish the biological significance of chelated proteins. Tetrapeptide fragments Cys-X-Y-Cys (X,Y = amino acid residues) are found in the metal binding sites of many metal thiolato proteins.¹⁸ These proteins include *C. pasteurianum* rubredoxin, *Spirulina plaensis* ferredoxin, *E. coli* aspartate carbamoyl transferase, and renal metallothionein.¹⁸ Spectroscopic characterizations of $\text{Fe}_4\text{S}_4^{2+}$ complexes of cysteine-containing tetrapeptides were determined using ^1H NMR and CD in a study of

electrochemical properties of the chelating tetrapeptide complexes.¹⁸ In this study, ¹H NMR was used to establish the chelation of Cys-X-Y-Cys to the [4Fe-4S] cluster by the observation of two sets of characteristic ¹H NMR signals of CysC_βH₂.¹⁸ Two peaks around 12-14 ppm (in Me₂SO-d₆ or dichloromethane-d₂) were observed in [4Fe-4S] complexes of tripeptides and dipeptides containing a cysteine residue. These peaks were the result of non-equivalent C_βH₂ protons that were contact-shifted by the Fe₄S₄²⁺ core through the C-S-Fe bond.¹⁸

The solvent dependence of ¹H NMR and CD spectra of [Fe₄S₄(Z-Cys-Gly-Ala-CysOMe)₂]²⁻ were interpreted as demonstrating flexible chelation of the peptide. Circular dichroism results supported chelating coordination of two cysteine-containing peptides to a single cluster.¹⁸ This experiment established that the invariant sequence around Fe₄S₄²⁺ in bacterial ferredoxins might play an important role in electron transfer, especially in influencing the direction of flow of electrons in biological electron-transfer chains.¹⁸

Cyclic Dipeptide or Protein Folding Secondary to Metal Ion Binding

Cyclic diglycine, the simplest cyclic dipeptide, exists in a planar ring conformation. Replacement of one or both of the glycines by an amino acid with a larger group changes the preferred conformation. When an aryl substituent was used in studies of 2,5-dioxopiperazine's (DOP's), three conformations of the DOP ring were observed: planar (Figure 3), flagpole boat (Figure 4), and bowsprit boat (Figure 5).¹⁹ Initially reported as responsible for the ring-shielding effects observed in NMR spectra, the flagpole conformation appears to be the most common for cyclic dipeptides with two aromatic sidechains, possibly as a result of attractive forces between the two rings. This

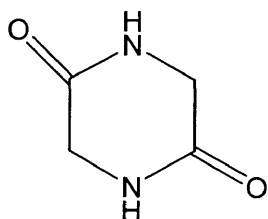


Figure 3: Planar conformation of DOP ring

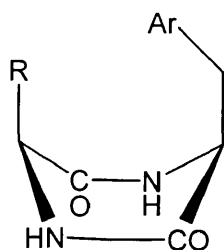


Figure 4: Flagpole boat conformation of DOP ring

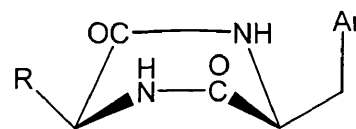


Figure 5: Bowspirit boat conformation of DOP ring

conformation is apparently less favored for non-aromatic substituents.¹⁹ In limited previous studies of metal binding by cyclic dipeptides, metal binding induced the flagpole conformation.¹⁹

The “folding” process to be investigated involves the cyclic dipeptide ring flip from the bowspirit structure, with the side chains pointing out, to the flagpole structure with the side chains both directed at a metal. Cyclic dipeptides with two metal binding groups, for example cyclo(L-histidyl-L-histidyl) and cyclo(L-methionyl-L-methionyl), will be compared to those with just one metal binding group. The side chains of the amino acids histidine (Figure 6) and methionine (Figure 7) are frequently bound to metals in proteins, while the side chain of alanine (Figure 8) is incapable of metal binding. Cyclo(L-histidyl-L-histidyl) (Figure 9) and cyclo(L-methionyl-L-methionyl) (Figure 10)

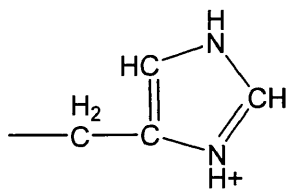


Figure 6: Histidine side chain

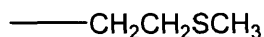


Figure 7: Methionine side chain

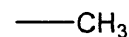


Figure 8: Alanine side chain

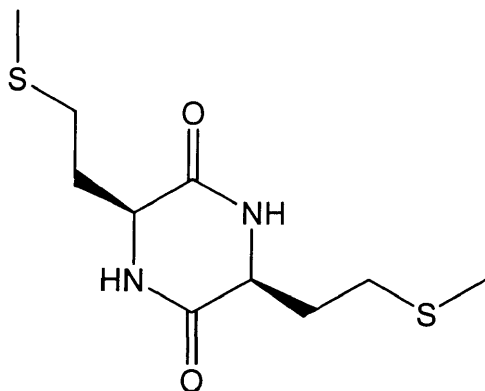


Figure 9: Cyclo(L-methionyl-L-methionyl)

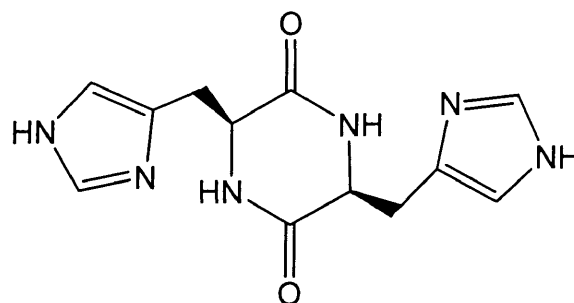


Figure 10: Cyclo(L-histidyl-L-histidyl)

are available in one step synthesis from commercially protected amino acids. Protected dipeptides containing two different amino acids were synthesized as precursors to cyclo(L-alanyl-L-methionyl) (Figure 11) and cyclo(L-alanyl-L-histidyl) (Figure 12).

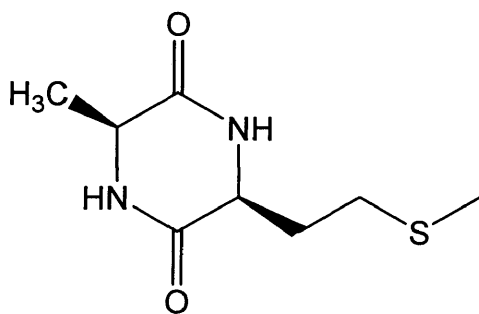


Figure 11: Cyclo(L-alanyl-L-methionyl)

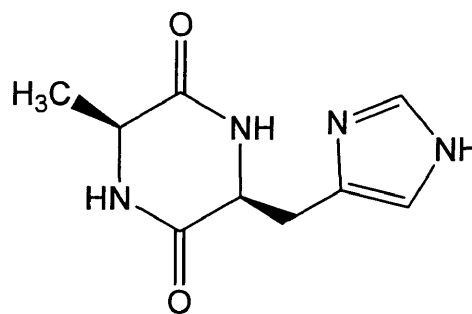


Figure 12: Cyclo(L-alanyl-L-histidyl)

Cyclic dipeptides will also be studied through solid-state NMR, in their solid, crystalline form and as guests in the hydrophobic cavities of cyclodextrin inclusion compounds. Controlling the host-guest intermolecular potential can be achieved by confining dipeptides in cyclodextrins of progressively larger cavity sizes. Successful inclusion of the cyclic dipeptide into a cyclodextrin will alter the ligand environment

thereby changing its dynamics, and thus changing the solid state NMR characterization of the dipeptide. The cyclic dipeptide cyclo(L-leucyl-D-prolyl) was chosen for use in this study because it has been previously characterized by X-ray crystallography and is biologically active. β cyclodextrin will be used to host the cyclo(L-leucyl-D-prolyl) (Figure 13) in a 1:2 ratio of guest:host. This study will also serve to complement related studies of leucine and cyclo(L-leucyl-L-glycyl).

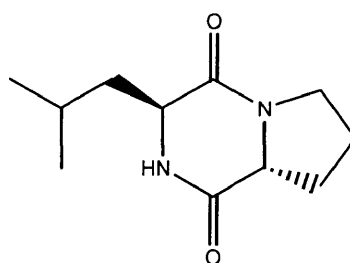


Figure 13: Cyclo(L-leucyl-D-prolyl)

EXPERIMENTAL

Unless otherwise noted all of the reagents and solvents used were commercially available. All syntheses were performed under argon, except for X-ray crystal growth, and organic products and crystals were purged with argon for storage. ^1H NMR was used to check the purity of all intermediates. The purity of ligands was confirmed using ^1H NMR and ^{13}C NMR spectroscopy. A Melt-Temp® melting point apparatus was used to obtain all melting points. Nuclear Magnetic Resonance Spectroscopy was performed on all samples using a Varian Mercury 400 MHz spectrometer and all chemical shifts are reported relative to tetramethylsilane. Elemental Analysis was performed by Atlantic Microlabs, Inc. A. Deer and J. Poutsma performed all mass spectrometry experiments.

Synthesis of N-(Benzyloxycarbonyl)-L-Alanyl-L-Histidyl Methyl Ester (ZAHOMe)

Both the N-benzyloxycarbonyl protected dipeptide and the cyclic dipeptide were prepared by modification of literature procedures.^{20,21} A solution of N-(benzyloxycarbonyl)-L-alanine (Z-AlaOH; 12.00 g, 8.95 mmol) in 50 mL of acetonitrile was prepared with stirring under argon. Dicyclohexylcarbodiimide (DCC; 1.84 g, 8.95 mmol) and then 4-nitrophenol (1.25 g, 8.95 mmol) were added to the Z-AlaOH solution. After stirring for approximately one hour, the precipitated DCU (dicyclohexylurea) was removed by vacuum filtration. The filtrate was added to a solution of L-histidine methyl ester (L-HisOMe; 2.17 g, 8.95 mmol) dissolved in acetonitrile (50 mL) and triethylamine

(2.45 mL, 17.90 mmol) that had been stirring for 5.5 hours. This reaction mixture was stirred under argon for 2 days.

Crude ZAHOMe was removed from solution via vacuum filtration and rinsed four times with 10 mL portions of acetonitrile, until the solid was no longer yellow, and then rinsed once with 20 mL of diethyl ether. The sample was sequentially suspended in 30 mL of chloroform, 30 mL of 0.5 M aqueous ammonia, and 30 mL of deionized water, with vacuum filtration between washings. The white solid was recrystallized from ethanol/ether. Crystals were isolated via vacuum filtration and then thoroughly dried under vacuum overnight, yielding 1.08 g of white ZAHOMe crystals. **MP:** $^1\text{H NMR}$: (DMSO- d_6) (Appendix 1): δ 8.31 (d, $J = 8.2$ Hz, H_c), 7.53 (s, H_i), 7.49 (d, $J = 9.3$ Hz, H_f), 7.36 (m, $H_a H_{a'}$, $H_{a''}$), 6.83 (s, H_j), 5.02 (dd, $J = 12.9, 4.6$ Hz, H_b), 4.47 (q, $J = 7.2$ Hz, H_g), 4.08 (p, $J = 7.3, 8$ Hz, H_d), 3.57 (s, H_i), 2.38 (m, H_h), 1.20 (d, $J = 8.5$ Hz, H_e)

Synthesis of Cyclo(L-Alanyl-L-Histidyl) (cAH)

To remove the Z protecting group, ZAHOMe (1.08 g, 2.87 mmol) was hydrogenated (40 psi, H_2) with 10% palladium-carbon catalyst (0.107 g) in 50 mL of methanol for 6.5 hours. The methanol solution was vacuum filtered through a celite bed. The filtrate was refluxed under argon for 60 hours and the solvent was removed by rotary evaporation to produce a white solid. Cyclo-(L-alanyl-L-histidyl) was then recrystallized from methanol and dried under vacuum overnight producing 0.4866 g (2.34 mmol) of white cAH crystals (81% yield). **MP:** 244-247°C $^1\text{H NMR}$: (DMSO- d_6) (Appendix 2): δ 8.19 (s, H_c), 8.10 (s, H_f), 7.98 (s, H_i), 7.56 (s, H_b), 6.81 (s, H_a), 4.05 (t, $J = 6.8$ Hz, H_h), 3.81 (q, $J = 6.9$ Hz, H_e), 2.97 (dd, $J = 3.4, 11.2$ Hz, H_d), 2.86 (dd, $J = 6.0, 8.6$ Hz, $H_{d'}$),

0.97 (d, $J = 6.8$ Hz, H_g) ^{13}C NMR: (DMSO- d_6) (Appendix 4): δ 169.04, 167.73, 135.38, 133.41, 118.06, 55.35, 50.49, 30.69, 19.64 **Elemental Analysis:** Calculated for $(\text{C}_9\text{H}_{12}\text{N}_4\text{O}_2)_4 \cdot \text{CH}_3\text{OH}$: C, 51.38; H, 6.06; N, 25.91; O, 16.65 Found: C, 51.35; H, 5.81

Synthesis of Cyclo-(L-Histidyl-L-Histidyl) (cHH)

Cyclo(L-histidyl-L-histidyl) was prepared with modification of the literature procedure used by Abdehalden and associates.²² L-Histidine methyl ester dihydrochloride (5.00 g, 20.65 mmol) was dissolved in 100 mL of hot methanol and allowed to cool to room temperature. Sodium methoxide (4.99 mL of 30 wt % $\text{NaOCH}_3/\text{CH}_3\text{OH}$) was added to the room temperature solution. One minute later, 50 mL of diethyl ether was added. After approximately two minutes the NaCl that formed was removed via vacuum filtration. The filtrate was reduced to dryness via rotary evaporation. The residue was stirred in a 37°C oil bath for 8 days under argon. A white solid was removed from the solution by means of vacuum filtration, and washed with several 20 mL portions of cold methanol. Cyclo(L-histidyl-L-histidyl) was isolated by recrystallization from ultra pure deionized hot water. The cHH was further dried overnight in a vacuum oven at 100°C , yielding 355 mg of a white solid (12.5 % yield). **MP:** $269\text{-}278^\circ\text{C}$ (dec) ^1H NMR: (DMSO- d_6) (Appendix 3a): δ 7.98 (s, H_c), 7.58 (s, H_b), 6.78 (s, H_a), 3.98 (t, $J = 4.1$ Hz, H_e), 2.99 (dd, $J = 4.0, 15.0$ Hz, H_d'), 2.58 (dd, $J = 8.9, 6.4$ Hz, H_d) ^{13}C NMR: (DMSO- d_6) (Appendix 3b): δ 167.61, 135.53, 134.02, 117.96, 55.22, 31.03

Synthesis of N-(Benzyloxycarbonyl)-L-Alanyl-L-Methionyl Methyl Ester (ZAMOMe)

ZAMOMe and cAM were both prepared with modification to literature procedure.²³ N-(Benzyloxycarbonyl)-L-alanine (Z-AlaOH; 5.00 g, 22.39 mmol) was dissolved in approximately 100 mL of still dried tetrahydrofuran and cooled to -10°C in an ice/salt bath. N-methylmorpholine was added (2.46 mL, 22.39 mmol) to the cooled solution. L-Methionine methyl ester hydrochloride (L-MetOMe; 4.471g, 22.39 mmol) was suspended in approximately 50 mL of N,N-dimethylformamide (DMF). The DMF suspension was heated slightly to ensure saturation and cooled to room temperature. Isobutyl chloroformate (2.904 mL, 22.39 mmol) was added to the Z-AlaOH solution under a light stream of argon. In the next minute, triethylamine (3.06 mL, 22.39 mmol) was added to the cooled N,N-dimethylformamide solution. This N,N-dimethylformamide mixture was added to the tetrahydrofuran solution described above. This solution was stirred under argon for three days. Salts were removed by vacuum filtration, rinsing with tetrahydrofuran (THF) and the THF was removed via rotary evaporation. Ultra pure water (20mL) was added and the solution was extracted with methylene chloride (3 x 30 mL). The combined organics were dried with sodium sulfate and the solution was reduced via rotary evaporation to a colorless oil. Ultra pure water (100 mL) was added to the residue. Following two days of re Fridgeration, white N-(Benzyloxycarbonyl)-L-alanyl-L-methionyl methyl ester (ZAMOMe) crystals were removed via vacuum filtration and dried under vacuum overnight yielding 5.15 g (15.32 mmol) of ZAMOMe (68.4% yield). ¹H NMR: (DMSO-d₆) (Appendix 4): δ 8.24 (d, *J* = 11.6 Hz, H_c), 7.41 (d, *J* = 7.7 Hz, H_f), 7.34 (m, H_a, H_a', H_a''), 4.99 (s, 2 H_b), 4.39 (q, *J* =

7.5, 8.9 Hz, H_g), 4.07 (p, $J = 7.5, 6.8$ Hz, H_d), 3.62 (s, 3 H_k), 2.44 (m, H_i), 2.03 (s, 3 H_j), 1.99 (m, H_h), 1.20 (d, $J = 7.7$ Hz, H_e)

Synthesis of Cyclo(L-Alanyl-L-Methionyl) (cAM)

ZAMOMe (5.15 g, 15.32 mmol) was hydrogenated (40 psi, H₂) with 10% palladium-carbon catalyst (0.0575 g) in 100 mL of methanol for 18 hours. This solution was vacuum filtered through celite and the filtrate volume was reduced by rotary evaporation to produce a thick yellow oil. Crude L-alanyl-L-methionyl methyl ester (AMOMe) oil was refluxed with ~140 mL of toluene for 24 hours. Toluene was removed through rotary evaporation, and the resulting translucent yellow cAM crystals were dried under vacuum for ~18 hours, producing 3.46 g of crude cAM (78% crude yield). Cyclo(L-alanyl-L-methionyl) was recrystallized in 350 mL of ethyl acetate. The resulting crystals were vacuum filtered and dried overnight under vacuum, yielding 6.68% cAM (0.2314 g). Attempts to retrieve more cAM from the mother liquor were unsuccessful. **Mp:** 220-224°C **¹H NMR:** (DMSO-d₆) (Appendix 5a): δ 8.15 (d, $J = 8$ Hz, 2 H_e), 3.93 (t, $J = 5.1$ Hz, H_d), 3.88 (q, $J = 6.9$ Hz, H_g), 2.58 (m, H_b), 2.01 (s, H_a), 1.94 (m, H_c), 1.24 (d, $J = 6.9$ Hz, H_f) **¹³C NMR:** (DMSO-d₆) (Appendix 5b): δ 169.65, 168.29, 53.80, 50.51, 32.78, 29.49, 19.81, 15.26 **Elemental Analysis:** Calculated for C₈H₁₄N₂O₂S: C, 47.52; H, 6.93; N, 13.86. Found: C, 47.79; H, 7.00; N, 13.66.

Synthesis of N-(Benzyloxycarbonyl)-D-Prolyl-L-Leucyl Methyl Ester (ZPLOMe)

N-(Benzyloxycarbonyl)-D-proline (Z-ProOH; 2.00g, 8.02 mmol) was dissolved in ~20 mL of still dried THF and then cooled to -10°C, while stirring under argon. N-methylmorpholine (0.880mL, 8.02 mmol) was added to the reaction vessel. L-leucine methyl ester hydrochloride (1.457g, 8.02 mmol) was dissolved in ~20 mL of N, N-dimethylformamide (DMF). Isobutyl chloroformate (1.04 mL, 8.02 mmol) was then added to the Z-ProOH solution. In the next minute, triethylamine (1.09 mL, 8.02 mmol) was added to the DMF solution. The entire mixture was then added to the Z-ProOH reaction vessel and allowed to react for 4 days under argon. The formed salts were removed through vacuum filtration. The solvent was removed through rotary evaporation. The residue was dissolved in ~40 mL of chloroform and extracted with ultra pure deionized water (3 x 30 mL). The organic layer was dried with sodium sulfate, filtered and rotary evaporated. Crystallization of the resulting clear, yellow oil was induced by the addition of ~50 mL of 4°C ultra pure water. The crystals were removed via vacuum filtration and dried overnight in vacuo, resulting in 1.419 g (3.7 mmol, 46% yield) of ZPLOMe. ¹H NMR: (DMSO-d₆) (Appendix 6): δ 8.02 (s, H_g), 7.03 (m, H_a, H_{a'}, H_{a''}), 4.19 (t, J = 7.5 Hz, H_f), 4.00 (t, J = 6.9 Hz, H_h), 3.63 (s, H_b), 2.31 (s, H_i), 2.11 (m, H_i, H_j), 1.83 (m, H_d), 1.35 (m, H_c), 0.87 (dd, J = 3.5, 3.0 Hz, H_k)

Synthesis of N-(Benzyloxycarbonyl)-L-Leucine (Z-LeuOH)

L-leucine (1.00g, 7.62 mmol) was suspended in 20 mL of ultra pure deionized water. Two equivalents of triethylamine (2.1 mL, 15.2 mmol) and 10 mL of 95% ethanol were added to the L-leucine suspension. Solid N-(benzyloxycarbonyloxy)-succinimide

(1.89g, 7.62 mmol) was added to the reaction vessel. This mixture was allowed to stir under argon for two days. The colorless solution was concentrated by rotary evaporation. The residue was diluted with 50 mL of 100% ethanol and concentrated by rotary evaporation three times. The residue was then dissolved in 10 mL of chloroform and extracted three times with dilute HCl pH=2. The organics were dried with sodium sulfate, filtered, and concentrated through rotary evaporation. The resulting Z-LeuOH oil was dried in vacuo, yielding 1.612g (6.00 mmol, 78.7% yield). $^1\text{H NMR}$: (DMSO- d_6) (Appendix 7): δ 12.57 (s, H_h), 7.59 (d, $J = 9.2$ Hz, H_c), 7.35 (m, $\text{H}_a, \text{H}_a', \text{H}_a''$), 5.03 (s, H_b), 3.96 (s, H_d), 1.47 (m, H_e), 1.45 (m, H_f), 0.85 (dd, $J = 6.8, 4.9$ Hz, H_g)

Synthesis of N-(Benzyloxycarbonyl)-L-Leucyl-D-Prolyl Methyl Ester (ZLPOMe)

Z-LeuOH was dissolved in 75 mL of still dried THF and chilled to -10°C , while stirring under argon. N-methylmorpholine (0.598 mL, 6.00 mmol) and isobutyl chloroformate (0.778 mL, 6.00 mmol) were added to this mixture. Within one minute of adding the isobutyl chloroformate to the reaction vessel, triethylamine (0.826 mL, 6.00 mmol) was added to D-proline methyl ester hydrochloride (D-ProOMe; 0.776g, 6.00 mmol) dissolved in 35 mL of room temperature N,N-dimethylformamide (DMF). The entire D-ProOMe/ DMF mixture was then added to the reaction vessel and allowed to react, under positive argon pressure, for 10 days, at which point the resulting salts were removed through vacuum filtration. An extraction with ultra pure deionized water of the resulting Z-L-leucyl-D-prolyl methyl ester (ZLPOMe) dissolved in ~ 50 mL of chloroform followed and was repeated twice. Excess water was removed with the addition of sodium sulfate and the chloroform was removed via rotary evaporation. The

resulting yellow oil was dried overnight in vacuo yielding 1.9387g (5.15 mmol) of ZLPOMe (85.8% yield). ¹H NMR: (DMSO-d₆) (Appendix 8): δ 7.56 (s, H_c), 7.36 (m, H_a, H_{a'}, H_{a''}), 5.03 (s, H_b), 4.36 (t, J = 12.8 Hz, H_k), 4.25 (dd, J = 6.9, 8.5 Hz, H_d), 2.73 (s, H_l), 2.18 (m, H_h, H_i, H_j), 1.90 (m, H_e, H_f), 1.53 (m, H_h, H_i, H_j), 0.89 (m, H_g)

Synthesis of Cyclo(L-Leucyl-D-Prolyl) (cLP)

The N-benzyloxycarbonyl protecting group was removed from the linear dipeptides, ZLPOMe and ZPLOMe, via hydrogenation. ZLPOMe (1.9387 g, 5.15 mmol) was added to 0.1931 g of palladium over carbon (Pd/C) dissolved in ~50 mL of methanol. The mixture was allowed to react with 40 psi of hydrogen gas for 48 hours. Pd/C was removed from the mixture by vacuum filtration through celite. The resulting filtrate was then reduced to a concentrated oil of L-leucyl-D-prolyl methyl ester (LPOMe) via rotary evaporation* and dissolved in 100 mL of toluene. The LPOMe-toluene mixture was allowed to reflux for ~24 hours under argon. Toluene was removed through rotary evaporation and the remaining solid recrystallized in 50 mL of tetrachloroethylene. Off-white crystals were removed via vacuum filtration and dried overnight. From ZLPOMe: 26.3% cLP (0.3311 g, 1.577 mmol). **Mp:** 163-165°C ¹H NMR: (DMSO-d₆) (Appendix 9a): δ 7.97 (s, H_e), 4.17 (t, J = 8 Hz, H_c), 3.98 (t, J = 8 Hz, H_d), 2.09 (m H_f), 1.80 (m H_j, h, i), 1.34 (m H_b), 0.81 (q, J = 4 Hz, H_a). ¹³C NMR: (DMSO-d₆) (Appendix 9b): δ 170.99, 167.15, 59.21, 53.33, 45.63, 38.51, 28.21, 24.85, 23.62, 23.26, 22.68 **MS:** (H₂O:CH₃OH, 50:50 v/v) (Appendix 9c): 211, 194, 183, 181, 167, 155, 153, 138, 127, 86, 70

* Crude hydrogenation products, LPOMe and PLOMe, were also used in mass spectrometric analysis by J. Poutsma and A. Deer.

From ZPLOMe: 28.7 % cLP (0.4078 g, 1.94 mmol) **Mp:** 158-164°C **¹H NMR** (DMSO-*d*₆) (Appendix 10a): δ 8.02 (s, H_e), 4.19 (t, *J* = 8 Hz, H_c), 4.00 (t, *J* = 8 Hz, H_d), 2.11 (m, H_f), 1.82 (m, H_{g, h, i}), 1.34 (m, H_b), 0.86 (q *J* = 4 Hz, H_a) **¹³C NMR:** (DMSO-*d*₆) (Appendix 10b): δ 171.03, 167.13, 59.21, 53.35, 45.63, 38.55, 28.21, 24.86, 23.62, 23.27, 22.70 **Elemental Analysis:** Calculated for C₁₁H₁₈N₂O₂: C, 62.86; H, 6.57; N, 13.33. Found: C, 62.40; H, 8.64; N, 13.20.

Attempted cLP Integration into β Cyclodextrin by Slow Evaporation (Method I)

β cyclodextrin (1.94 g, 1.710 mmol) was suspended in 40 mL of ultra pure water. 180 mg (0.856 mmol) of cLP was added to the suspension and the mixture heated until all materials dissolved. The solution was filtered by gravity, to remove impurities and 4 mL of the resulting filtrate was transferred into each of four 8 mL vials. The vial caps were attached loosely enough to allow for evaporation to occur. The remaining filtrate was transferred into a 50 mL Erlenmeyer flask and covered with a Kimwipe. The vials and Erlenmeyer were allowed to sit, undisturbed for three weeks at which time clear crystals were harvested and sent for elemental analysis. **MP:** 270-275°C **Elemental Analysis:** Calculated for C₉₅H₁₅₈O₇₂N₂: C, 46.00; H, 6.42; N, 1.13; O, 46.44. Found: C, 39.26; H, 6.75; N, 0.00 – consistent with βCD (C₄₂H₇₀O₃₅ – Calculated: C, 40.44 H, 6.23 O, 49.34).

Attempted cLP Integration into β Cyclodextrin by Lyophilization (Method II)

β cyclodextrin (325 mg, 0.286 mmol) was suspended in 5 mL of ultra pure water. cLP (30 mg, 0.143 mmol) was added to the suspension and the mixture heated until the solution became clear. The solution was gravity filtered into an 200 mL roundbottom flask and frozen by rotating the roundbottom in a liquid nitrogen bath. The frozen mixture was then placed on a Labonco Freeze-Dry System/Freezone® 4.5 to dry overnight, resulting in a white powder, 65% yield (230 mg, 0.0927 mmol). **MP:** 275-285 °C **Elemental Analysis:** Calculated for $C_{95}H_{158}O_{72}N_2$: C, 46.00; H, 6.42; N, 1.13; O, 46.44. Found: C, 42.84; H, 6.72; N, 1.07; O, 49.37.

Preparation of NMR solutions for NMR titrations of cMM and $Hg(ClO_4)_2$

A 142 mM stock solution of cMM (0.0746 g, 0.0832 mmol) in DMSO- d_6 was prepared in a 2 mL volumetric. Separately, a 20 mM stock solution of mercury perchlorate (9.07 mg, 0.02 mmol) was prepared in a 1 mL volumetric. Solutions with metal-to-ligand ratios of 0.0156, 0.0208, 0.0313, 0.0625, 0.125, 0.25, 0.50, 1.0, 1.25, 1.50, and 2.0 were prepared from the stock solutions and DMSO- d_6 . To prepare each metal-to-ligand ratio, 65 μ L aliquots of the 20 mM $Hg(ClO_4)_2$ -DMSO- d_6 stock solution were placed in NMR tubes and diluted with varying amounts of cMM and DMSO- d_6 to obtain total volumes of 650 μ L, yielding 2mM of Hg(II) in each tube.

Preparation of NMR solutions for NMR titrations of cAM and Hg(ClO₄)₂

A 142 mM stock solution of cAM (57.3 mg, 0.283 mmol) in DMSO-d₆ was prepared in a 2 mL volumetric. A 20 mM solution of Hg(ClO₄)₂ (9.07 mg, 0.02 mmol) in DMSO-d₆ was prepared in a 1 mL volumetric. Solutions with metal-to-ligand ratios of 0.156, 0.0208, 0.0313, 0.125, 0.25, 0.50, 1.00, 1.25, 1.50, 2.00 were prepared from the stock solutions and DMSO-d₆. To prepare each metal-to-ligand ratio, 65 μL aliquots of the 20 mM Hg(ClO₄)₂-DMSO-d₆ stock solution were placed in NMR tubes and diluted with varying amounts of cAM and DMSO-d₆ to obtain total volumes of 650 μL, yielding 2mM of Hg(II) in each tube.

Preparation of NMR solutions for NMR titrations of cAH and Hg(ClO₄)₂

A 17.7 mM stock solution of cAH (7.65 mg, 0.0104 mmol) in DMSO-d₆ was prepared in a 2 mL volumetric. Separately, a 20 mM stock solution was prepared with Hg(ClO₄)₂ (9.07 mg, 0.02 mmol) in DMSO-d₆ in a 1 mL volumetric. Solutions with metal-to-ligand ratios of 0.125, 0.25, 0.375, 0.50, 0.625, 0.75, 0.825, 1.0, 1.125, 1.25, 1.375 were prepared from the stock solutions and DMSO-d₆. To prepare each metal-to-ligand ratio, 65 μL aliquots of the 20 mM Hg(ClO₄)₂-DMSO-d₆ stock solution were placed in NMR tubes and diluted with varying amounts of cAH and DMSO-d₆ to obtain total volumes of 650 μL, yielding 2mM of Hg(II) in each tube.

Preparation of NMR solutions for NMR titrations of cHH and Hg(ClO₄)₂

A 17.7 mM stock solution of cHH (9.70 mg, 0.0104 mmol) in DMSO-d₆ was prepared in a 2 mL volumetric. Separately, a 20 mM stock solution of Hg(ClO₄)₂ (9.07

mg, 0.02 mmol) in DMSO-d₆ was prepared in a 1 mL volumetric. Solutions with metal-to-ligand ratios of 0.125, 0.25, 0.375, 0.50, 0.625, 0.75, 0.825, 1.0, 1.125, 1.25, 1.375 were prepared from the stock solutions and DMSO-d₆. To prepare each metal-to-ligand ratio, 65 μL aliquots of the 20 mM Hg(ClO₄)₂-DMSO-d₆ stock solution were placed in NMR tubes and diluted with varying amounts of cHH and DMSO-d₆ to obtain total volumes of 650 μL, yielding 2mM of Hg(II) in each tube.

Preparation of NMR solutions for NMR titrations of cHH and Cd(ClO₄)₂•H₂O

A 17.7 stock solution of cHH (9.70 mg, 0.0104 mmol) in DMSO-d₆ was prepared in a 2 mL volumetric. A 20 mM stock solution of cadmium perchlorate hydrate (6.22 mg, 19.98 μmol) in DMSO-d₆ was prepared in a 1 mL volumetric. Solutions with metal-to-ligand ratios of 0.125, 0.25, 0.375, 0.50, 0.625, 0.75, 0.875, 1.0, 1.125, 1.25, 1.50 were prepared from the stock solutions and DMSO-d₆. To prepare each metal-to-ligand ratio, 65 μL aliquots of the 20 mM Cd(ClO₄)₂•H₂O-DMSO-d₆ stock solution were placed in NMR tubes and diluted with varying amounts of cHH and DMSO-d₆ to total volumes of 650 μL, yielding 2mM of Cd(II) in each tube.

RESULTS AND DISCUSSION

I. ORGANIC SYNTHESSES

Synthesis of Cyclo(L-Alanyl-L-Histidyl)

The synthesis of cAH was a multistep process. First, it was necessary to synthesize the intermediate Z-L-alanine-p-nitrophenol ester by adding dicyclohexylcarbodiimide (DCC) and then 4-nitrophenol to a solution of Z-L-alanine dissolved in acetonitrile. DCC is a carboxy group activating reagent used widely in peptide synthesis.²⁴ The DCC hydrates, forming dicyclohexylurea (DCU), which is insoluble in acetonitrile. Since DCU cannot be readily separated from Z-L-alanyl-L-histidyl methyl ester (ZAHOMe) by recrystallization, it was necessary to remove it by vacuum filtration prior to combining with L-histidine methyl ester.

Triethylamine was added to L-histidine methyl ester dihydrochloride dissolved in acetonitrile. The triethylamine neutralized the dihydrochloride salt from L-histidine methyl ester because of the greater basicity of triethylamine over histidine. Removing the dihydrochloride from L-histidine methyl ester permitted coupling of L-histidine methyl ester with Z-L-alanine-p-nitrophenol ester. This coupling reaction produced ZAHOMe, the result of amide bond formation between the N terminus of histidine and the C terminus of Z-AlaOH. The reaction proceeded because the amide bond is more stable than the existing ester bond between the C terminus of Z-AlaOH and the nitrophenol group.

The next step in cAH synthesis involved removing the N-(benzyloxycarbonyl) or Z group from the N terminus of alanine. Hydrogenation of ZAHOMe with a palladium on carbon catalyst in methanol removed the Z group, yielding AHOMe. AHOMe was then refluxed in methanol for approximately 60 hours to facilitate the transesterification reaction resulting in cAH. Purification, achieved by recrystallization in methanol, yielded 81% cAH (Figure 14).

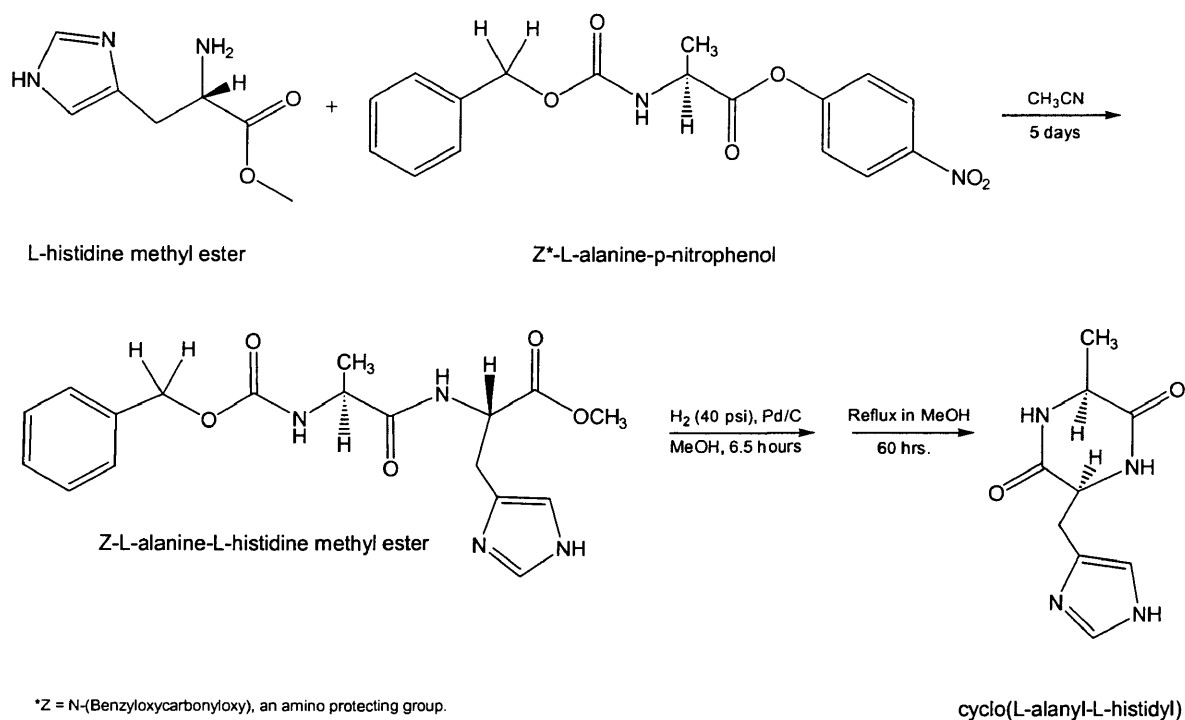


Figure 14: Synthesis of Cyclo(L-Alanyl-L-Histidyl)

Synthesis of Cylco(L-Histidyl-L-Histidyl)

Sodium methoxide was used to generate free amines from the commercially available dihydrochloride salt of L-histidine methyl ester. The cyclic dipeptide was formed from the linear dipeptide produced through an initial intermolecular nucleophilic attack of an amine onto the carbonyl of a methyl ester and elimination of methanol.

Unimolecular cyclization of the dipeptide methyl ester through intramolecular nucleophilic attack produced the cyclic dipeptide. Recrystallization from water produced cHH in 12.5% yield (Figure 15).

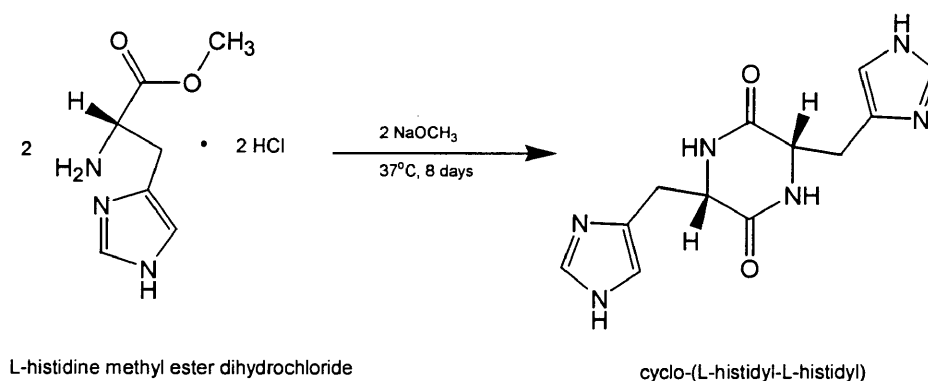


Figure 15: Synthesis of Cyclo(L-Histidyl-L-Histidyl)

The cyclic dipeptide is the major product of this reaction, despite the existence of several simultaneous and competing reactions. First, the six-membered ring structure of cHH is more stable than any smaller or larger ring structures that could form. Also of importance is the close proximity of the carbonyl and amine in the dipeptide, which favors internal attack over intermolecular attack. Further, this reaction is thermodynamically favored by the greater stability of amides over esters.

Synthesis of Cyclo(L-Alanyl-L-Methionyl)

The synthesis of cAM requires the preparation of several intermediates. ZAMOMe, the first of these intermediates, was synthesized via a multistep addition reaction. First, triethylamine was added to a solution containing DMF and L-methionine methyl ester dihydrochloride to neutralize the dihydrochloride salt. In a separate vessel,

N-methylmorpholine and isobutyl chloroformate were added to Z-AlaOH to facilitate the addition of Z-AlaOH to L-methionine. In this reaction, N-methylmorpholine was added to facilitate coupling between Z-AlaOH and isobutyl chloroformate by neutralizing the hydrochloric acid formed. The two solutions were then combined within one minute of having added isobutyl chloroformate to the Z-AlaOH solution, producing ZAMOMe. This coupling reaction was driven by the formation of an amide bond, which is more stable than the existing Z-L-alanyl-isobutyl formate ester bond.

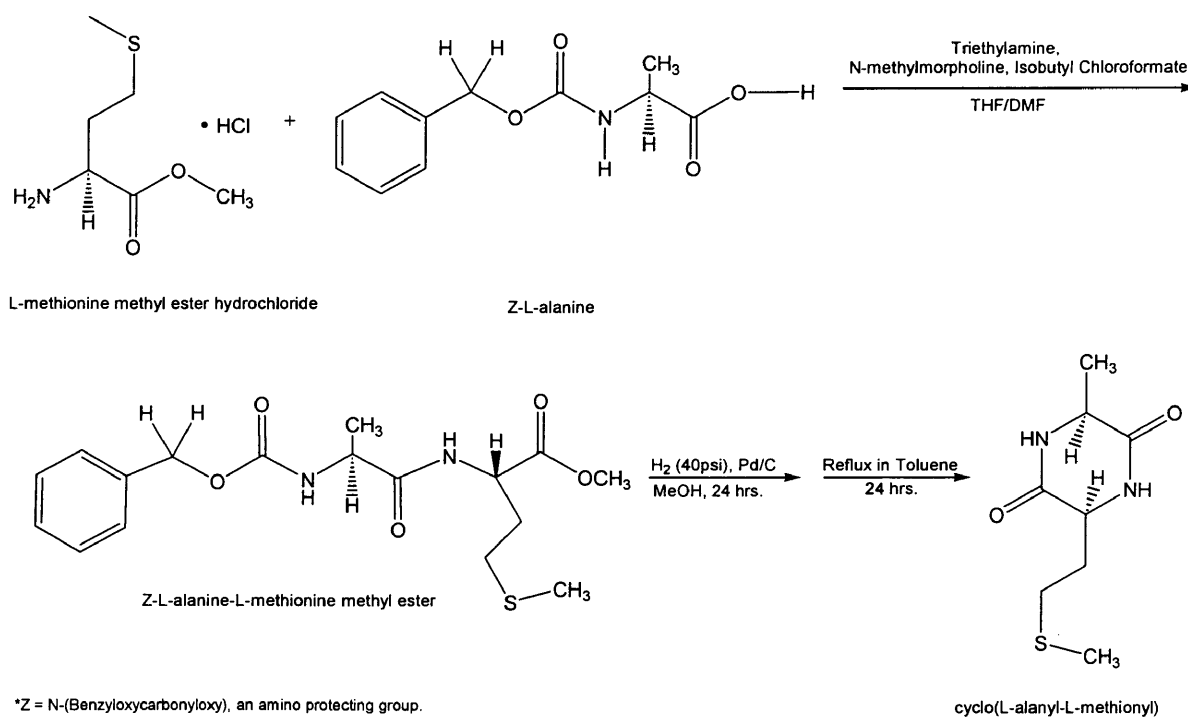


Figure 16: Synthesis of Cyclo(L-Alanyl-L-Methionyl)

The next intermediate in the synthesis of cyclo(L-alanyl-L-methionyl) was AMOMe. Hydrogenation of ZAMOMe over a Pd/C catalyst was used to remove the N-

(benzyloxycarbonyl) group (Z), which was protecting the N terminus of the dipeptide. This reaction was favored, as a carbamate bond is subject to reduction much more readily than an amide bond. After 24 hours of hydrogenation in a methanol solution, AMOMe was produced. To facilitate transesterification, the AMOMe was refluxed in toluene for 24 hours. Recrystallization from ethyl acetate yielded 7% cAM (Figure 16). Attempts to obtain more product from the filtrate were unsuccessful.

Synthesis of Cyclo(L-Leucyl-D-Prolyl)

The synthesis of cLP is very similar to that of cAM. The major difference between the two syntheses is the need to couple N(benzyloxycarbonyloxy) succinimide to L-leucine in the synthesis of cLP, whereas commercially available Z-L-AlaOH was used in the synthesis of cAM. The reason for this additional step is the future interest in synthesizing cLP using labeled leucine.

Once Z-LeuOH had been adequately dried, the coupling reaction between Z-L-leucine and isobutyl chloroformate was prepared. N-methylmorpholine was added as a base to facilitate coupling between Z-L-leucine and isobutyl chloroformate, to form Z-L-leucine isobutyl formate. Z-L-leucine isobutyl formate was then combined with L-proline methyl ester that was treated with triethylamine to remove the hydrochloride group from the amino acid. The resulting major product was ZLPOMe.

ZLPOMe was then hydrogenated with a palladium over carbon catalyst in methanol to remove N-(benzyloxycarbonyl), the N terminus protecting group. Hydrogenation for 48 hours yielded LPOMe, which was refluxed in toluene. After 24 hours of refluxing, the toluene solution was reduced via rotary evaporation and the

resulting solid was recrystallized from tetrachloroethylene, yielding 26% cLP (Figure 17).

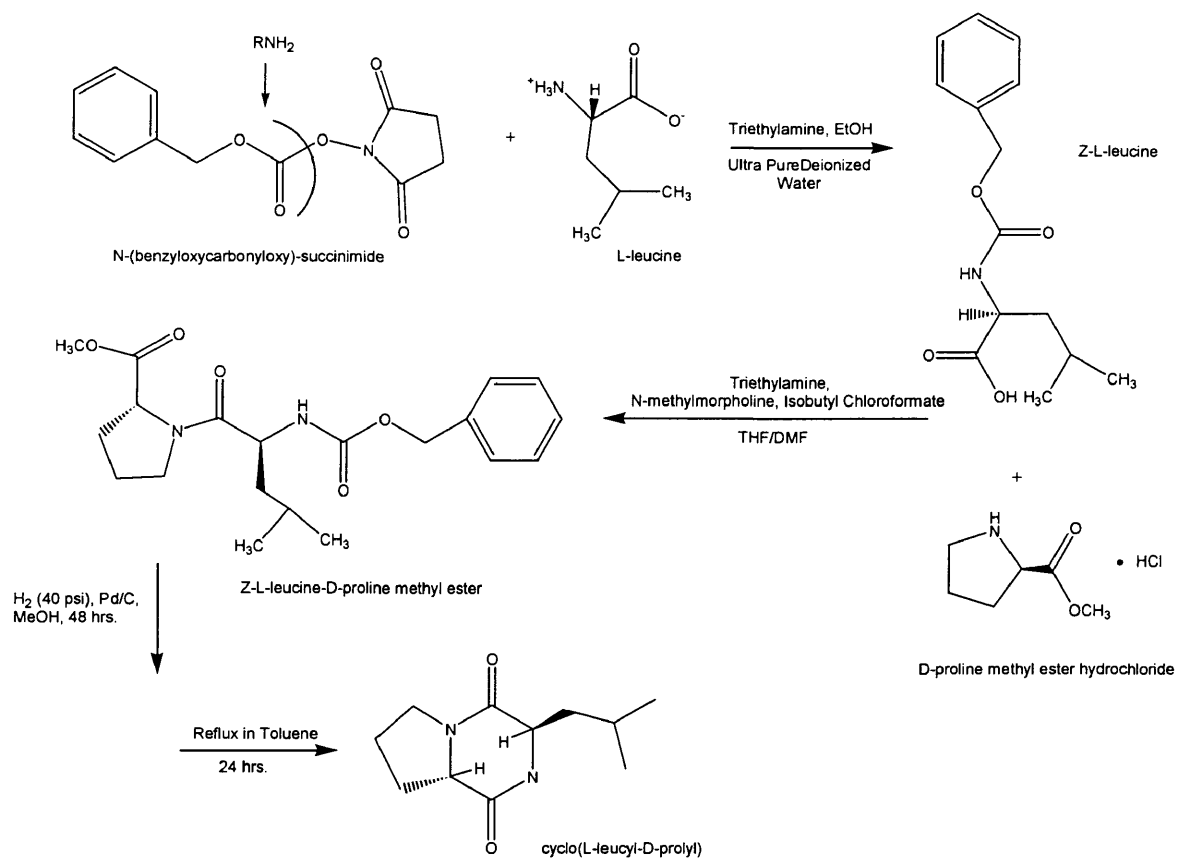


Figure 17: Synthesis of Cyclo(L-Leucyl-D-Prolyl).

II. MASS SPECTROMETRY ANALYSIS OF CYCLO(L-LEUCYL-D-PROLYL)

J. Poutsma and A. Deer conducted all mass spectrometry experiments using a quadrupole ion trap instrument (Finnigan LCQ-Deca™) fitted with an external electrospray ionization source. Dilute solutions (*ca.* 5×10^{-3} and 5×10^{-4} M) of the cyclic/linear dipeptide in slightly acidified (1% acetic acid) H₂O:CH₃OH (50:50 v/v) were directly infused into the mass spectrometer at flow rates in the range of 5-50 μ L/min. A typical mass spectrum of cLP is shown in Appendix 9c. Ions with the mass-to-charge ratio of the singly protonated dipeptide were isolated with a typical isolation width of 4-5 amu. The mass-selected ions were subjected to collision-induced dissociation with the background helium buffer gas serving as the target. Typical activation energies were in the range of 10-15 V (peak-to-peak, lab frame) and the activation time was 30 μ s. Product ion scans were then collected using the resonance ejection method. The process of ion isolation / fragmentation was repeated to give MS³, MS⁴, and MS⁵ spectra.

Cyclo(L-leucyl-D-prolyl) was isolated and fragmented. The information presented in Figure 17 depicts the suspected fragmentation pattern of the cyclic dipeptide.

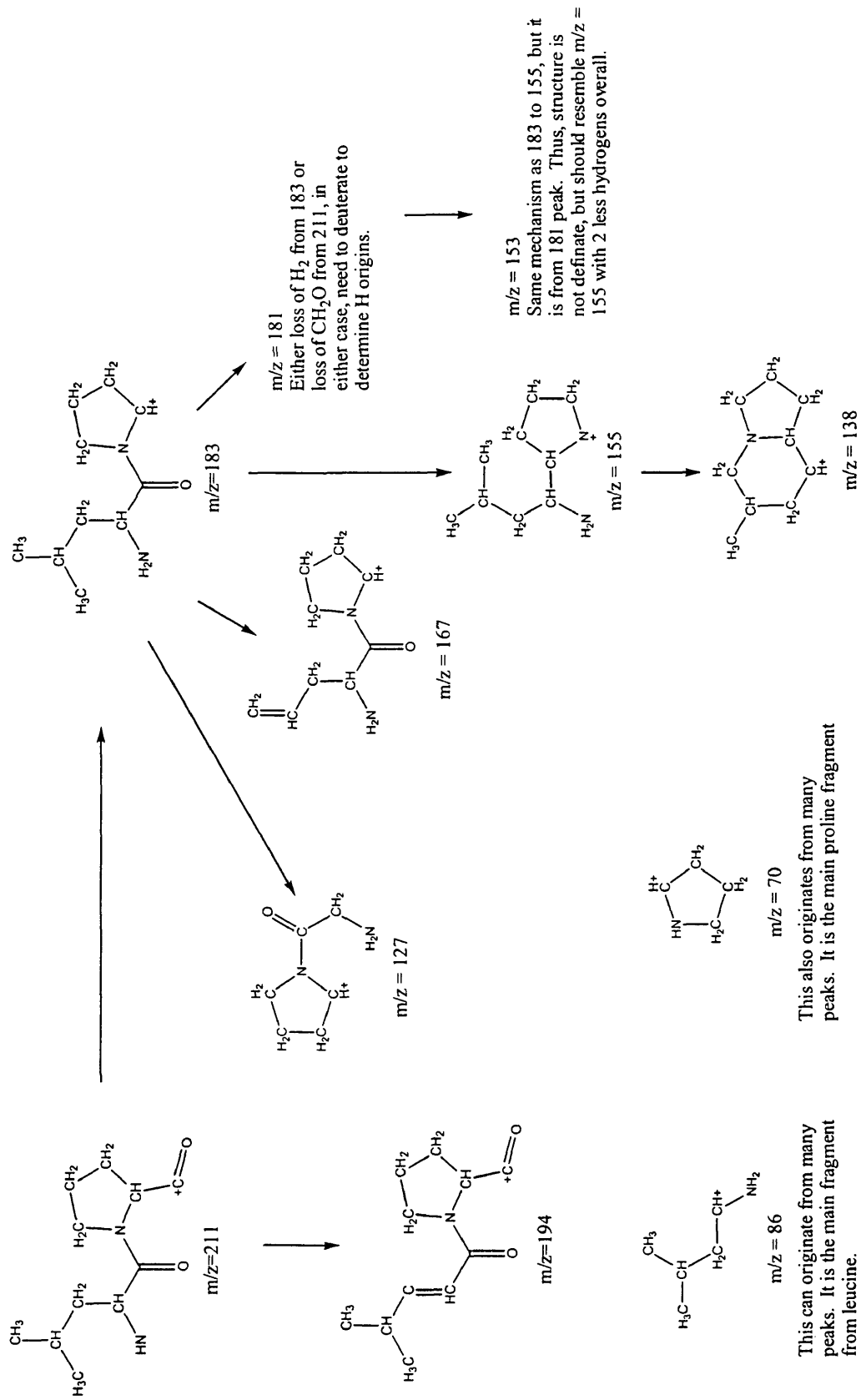


Figure 18: Mass spectrometric fragmentation of cLP.

III. CYCLO(L-LEUCYL-D-PROLYL) INTEGRATION INTO β CYCLODEXTRIN

Integration of cyclo(L-leucyl-D-prolyl) into β cyclodextrin (β CD) was attempted by two methods, both based on the procedure outlined by Brett and associates.²⁵ In one method (Method I), the cLP and β CD were combined and X-ray quality crystals were obtained by slow evaporation of the 1:2 cLP: β CD solution. However, elemental analysis of the crystals indicated isolation of pure β CD.

Prior to harvesting the crystals grown in Method I, there was concern β CD water inclusion in the crystalline structure of the complex would present a problem, thus Method II was proposed. In this method, the same procedure was used to combine cLP and β CD, the solution of which was then lyophilized. Using the lyophilization method we were able to prepare a powder with reasonable nitrogen content, suggesting the presence of cLP. However, the elemental analysis of this sample was not consistent with a hydrate of 1:2 cLP: β CD. These results combined with the elemental analysis characterization of the crystals produced in Method I, suggest that cLP is not intercalating inside the β CD as desired. This may indicate that the cavity was either too large or too small. The cLP may also be interacting with the exterior as opposed to the interior of the β CD cavity. Future attempts at cLP integration into a cyclodextrin are warranted, but should be attempted with α and γ cyclodextrin. These cyclodextrins are larger and smaller than β CD, and integration into either one would be adequate for solid-state NMR studies.

IV. NMR SOLUTION-STATE STUDIES OF HG(II) COORDINATION

Solution-State Investigations of Cyclo(L-Methionyl-L-Methionyl)

A series of solutions in which the Hg:cMM ratio was increased from 0 (free ligand) to 2:1 with 2 mM Hg(II) were prepared in DMSO-d₆. Proton NMR was performed on these solutions at room temperature. Figure 19 depicts the free ligand cMM with proton assignments. Figure 20 shows a plot of chemical shift vs. metal-to-ligand ratio of hydrogen atoms H_e, H_d, H_b, H_a, and H_g. Figure 21 shows a stacked plot of proton NMR spectra at selected metal-to-ligand ratios.

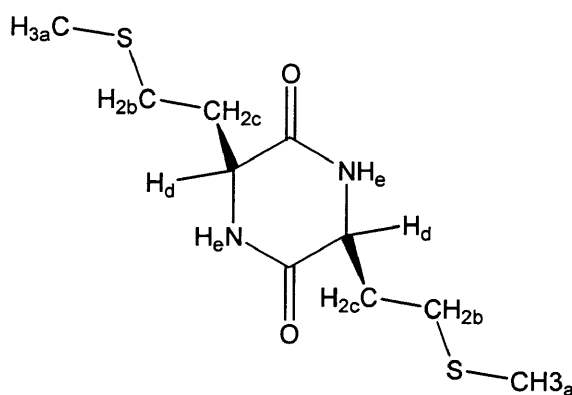


Figure 19: cMM

The metal-to-ligand ratios 0.0156, 0.0208, 0.0313, 0.0625, 0.125, 0.25, 0.5, 1.0, 1.25, and 1.50 were selected for to investigate the formation of 1:1 and 1:2 Hg(II):cMM complexes. At the [Hg]/[cMM] ratio 0.0313, two small peaks (H_b' and H_b'') are observed at 3.39 ppm and 2.47 ppm. These peaks increase in intensity, but remain at the same chemical shift over the course of the study. This suspicious behavior may be explained as the two H_b protons becoming prochiral in the presence of Hg(II) and appearing at different resonances. This was difficult to assess secondary to the presence of broad

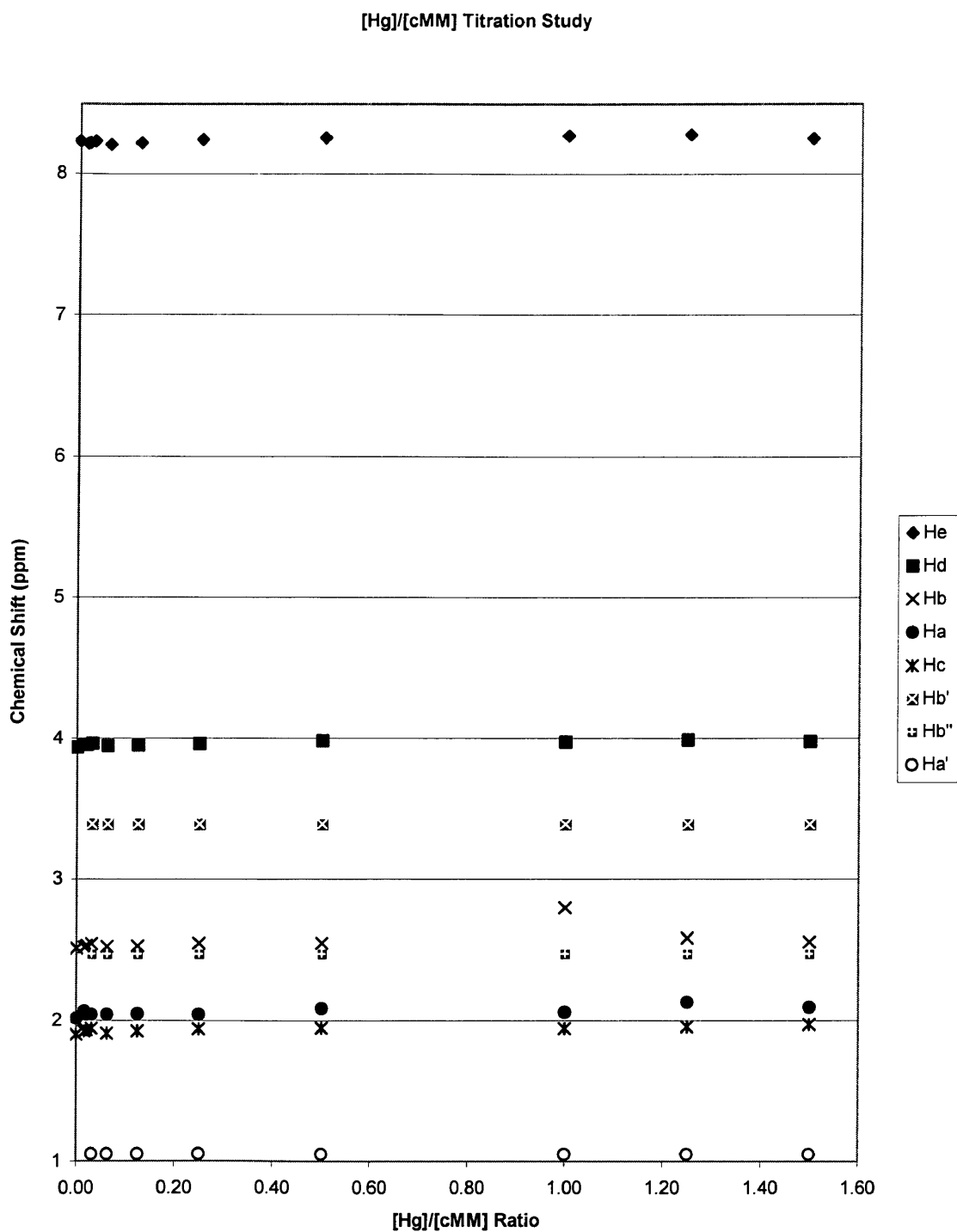


Figure 20: Chemical shifts of protons H_e, H_d, H_b, H_{b'}, H_{b''}, H_a, H_{a'}, and H_g in cMM in the presence of Hg(ClO₄)₂ as a function of metal-to-ligand ratio in DMSO-d₆ at room temperature. Total metal concentration was 2 mM.

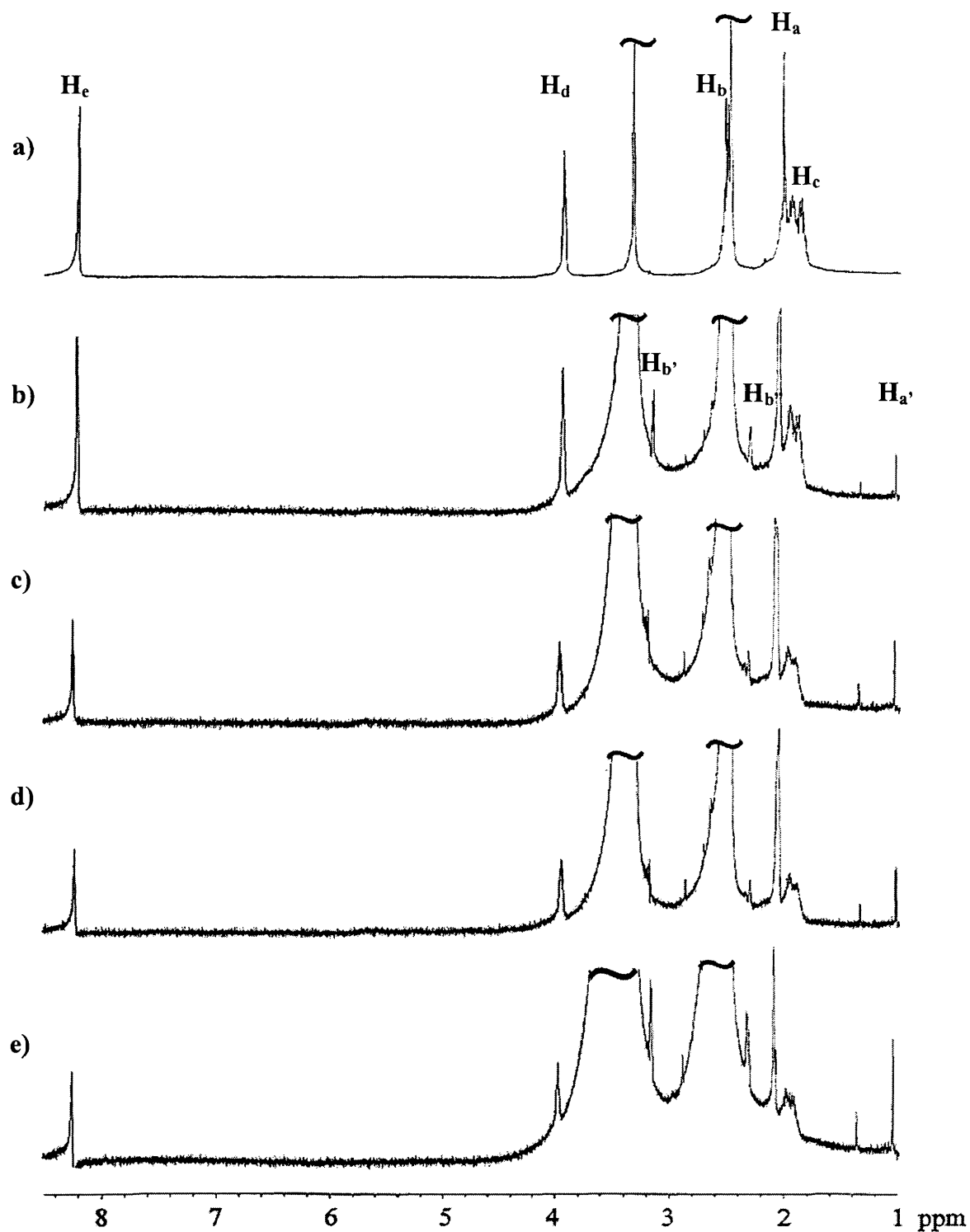


Figure 21: Stack plot of several ^1H NMR spectra of cMM in the presence of $\text{Hg}(\text{ClO}_4)_2$ at room temperature in DMSO-d_6 . Total metal concentration was 2 mM. Metal-to-ligand ratios = a) 0.0156, b) 0.25, c) 0.50, d) 1.0, e) 1.25.

water and DMSO-d₆ peaks in the same region of the spectrum. A third peak (H_{a'}) also appeared at the 0.0313 ratio. This peak, a singlet, appeared at 1.05 ppm and remained at that resonance throughout the rest of the study. It is possible that this peak is the methyl peak of a Hg:cHH complex. The noticeable broadening of H_a beginning at the 0.25 Hg:cMM ratio and then the sudden sharpening of the peak at the 1.0 ratio of Hg:cMM, was also of interest. This broadening might be an indication of possible exchange occurring between the H_a proton of free ligand and the H_a proton of a mercury complex, possibly a 1:2 complex since the change occurs suddenly at the 1.0 ratio. The sharpening of H_a may be secondary to the decrease in available free ligand for exchange at the 1.0 ratio.

These interpretations are speculative, especially since no ¹H change in chemical shift of the protons H_c, H_d, and H_e was observed. Since the methionyl side chain is commonly involved in binding divalent metal ions *in vivo*, one would expect to observe either a change in the chemical shift of the methionyl protons (especially H_a and H_b) or observe the appearance of new peaks, representative of some Hg(II):cMM complex. The appearance of new peaks H_{b'}, H_{b''}, and H_{a'}, may be suggestive of this Hg(II):cMM complex forming. However, while cMM is reported to complex in a 1:2 ratio with Ag(I), *in vitro*, our observations neither support nor refute this.²⁶ Thus the limited availability of previous NMR studies and the speculative nature of our observations warrant further NMR evaluation of cMM and Hg(II).

Solution-State Investigations of Cyclo(L-Alanyl-L-Methionyl)

Since the changes observed in the Hg:cMM titration study did not definitively suggest the presence of a Hg(II):cMM complex, a repeat titration study that substituted cAM for cMM was proposed. The cyclic dipeptide cAM was chosen because it has an alanine side chain in place of one of the methionine side chains of cMM, and alanine is incapable of metal binding. Thus, it was expected that the methionyl protons would exhibit the same changes as observed in the previously discussed Hg:cHH titration study, while the alanyl protons would not exhibit any changes over the course of the study.

A series of solutions in which the Hg:cAM ratio was increased from 0 (free ligand) to 2:1 with 2 mM mercury perchlorate were prepared in DMSO- d_6 . Proton NMR was performed on these solutions at room temperature. Figure 22 shows a plot of chemical shift vs. metal-to-ligand ratio of selected hydrogen atoms. Figure 23 shows a stacked plot of proton NMR spectra at selected metal-to-ligand ratios. Figure 24 shows cAM with proton assignments.

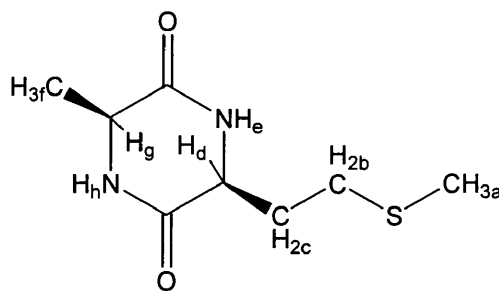


Figure 24: cAM

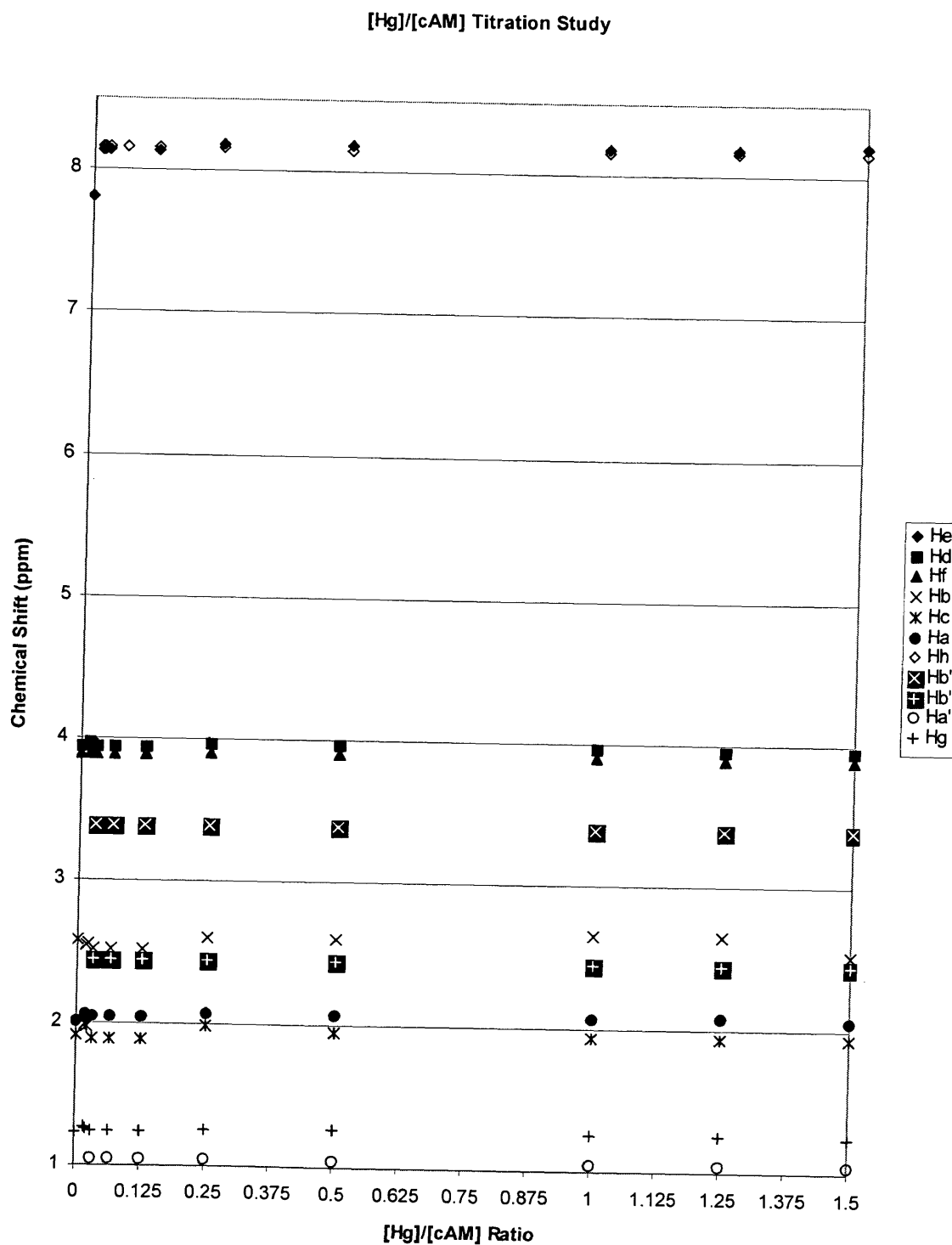


Figure 22: Chemical shifts of protons H_e, H_h, H_f, H_d, H_b, H_{b'}, H_{b''}, H_c, H_a, H_{a''}, and H_g in cAM in the presence of Hg(ClO₄)₂ as a function of metal-to-ligand ratio in DMSO-d₆ at room temperature. Total metal concentration was 2 mM.

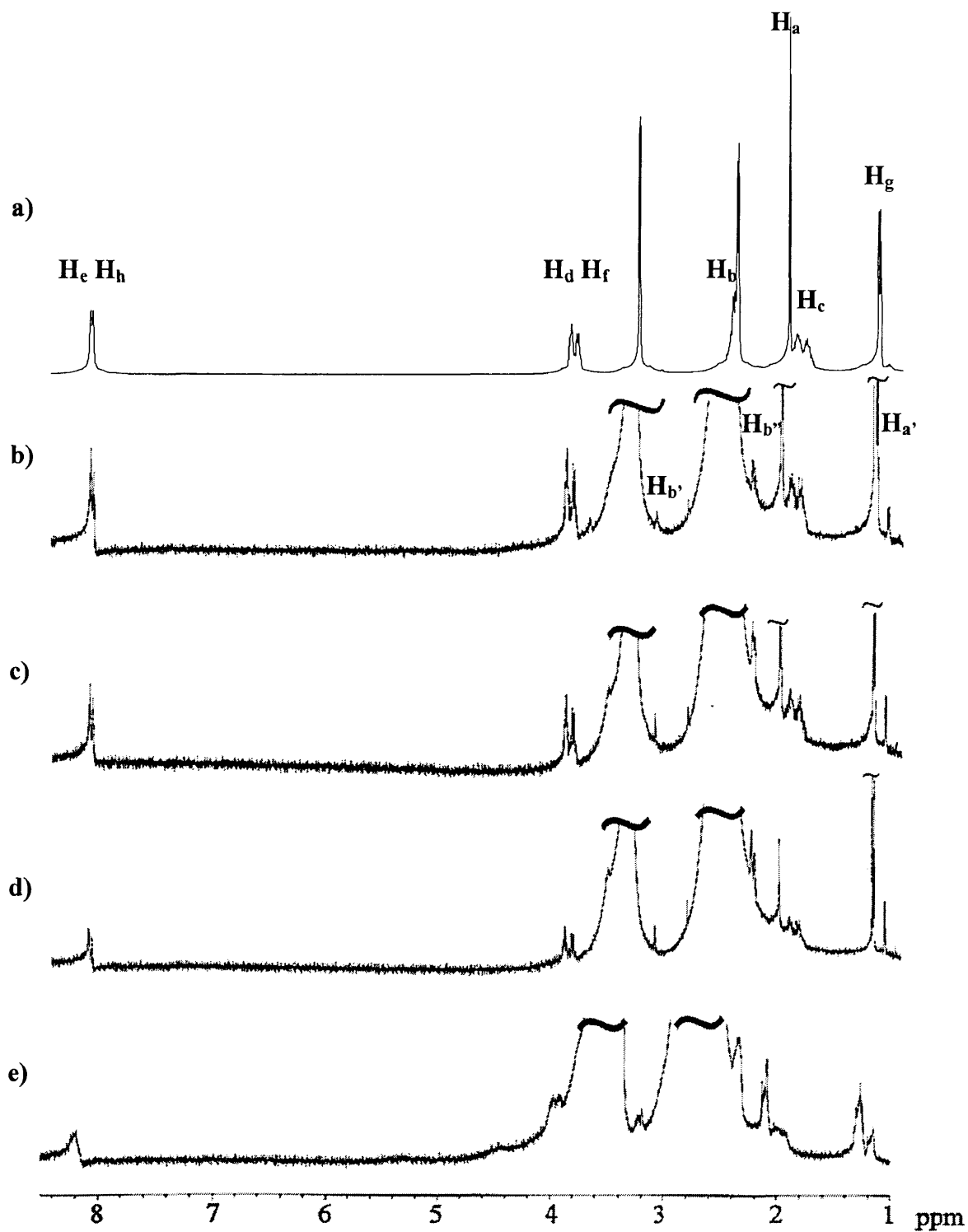


Figure 23: Stack plot of several ^1H NMR spectra of cAM in the presence of $\text{Hg}(\text{ClO}_4)_2$ at room temperature in DMSO-d_6 . Total metal concentration was 2 mM. Metal-to-ligand ratios = a) 0.0156, b) 0.25, c) 0.50, d) 1.0, e) 1.25.

The methionyl side chain is commonly involved in binding divalent metal ions *in vivo* and it was expected that the greatest effects of mercury(II) on cAM would be demonstrated by a change to the resonances for H_a, H_b, H_c, H_d, and H_e. As observed in the Hg(II):cMM titration study, two peaks appear at the Hg(II):cAM ratio of 0.0313 at 3.40 ppm and 2.45 ppm. This behavior suggests that the methylene protons (H_b) become prochiral in the presence of Hg(II) because the formation of a Hg(II):cAM complex changes the effective environment. These peaks increase in intensity but remain at the same chemical shift over the course of the study. Also of interest is the appearance of a new singlet (H_a') at 1.05 ppm at the 0.0313 Hg(II):cAM ratio. This peak increases in intensity throughout the remainder of the study, while H_a is noticed to decrease in intensity throughout the remainder of the study. This intensity change between H_a and H_a' suggests the formation of an Hg(II):cAM complex. The broadening of the amide peaks at 8.155 ppm (H_h) and 8.182 ppm (H_e) is also interesting, as it suggests the occurrence of exchange, a process that occurs on a time scale comparable to the NMR time scale or the frequency difference between nuclear environments. Finally, H_a broadened at the ratios 0.25 and 0.5, and then sharpened at ratios above 0.5, only to broaden again above 1.0. The change in broadening at the 0.5 ratio of Hg(II):cAM may suggest the formation of a 1:2 Hg(II):cAM complex, while the change above 1.0 may be suggestive of 1:1 complex formation. These interpretations are merely speculative, as concrete evidence for such interactions has not been observed.

The resonances for the alanyl protons, H_f and H_g were nearly unchanged throughout the series. The results of this study support the findings of the previously discussed Hg(II):cMM titration study in that Hg(II) is suggested to interact with the

sulfur of methionine. However the exact interaction and complex formation will not be fully understood and known without further NMR studies and X-ray analysis.

Solution-State Investigations of Cyclo(L-Hisidyl-L-Histidyl)

A series of solutions in which the Hg:cHH ratio was increased from 0 (free ligand) to 1.375:1 with 2 mM mercury perchlorate was prepared in DMSO- d_6 . Proton NMR was performed on these solutions both at room temperature and at 20°C. Figure 25 shows a plot of chemical shift vs. metal-to-ligand ratio of selected hydrogen atoms in the imidazole region. Figure 26 shows a stacked plot of proton NMR spectra at selected metal-to-ligand ratios. Table 1 and 2 show proton chemical shifts of the initial and repeat metal-to-ligand titration studies of Hg:cHH.

The histidine side chain is a common binding group for divalent metal cations *in vivo*. cHH (Figure 27) has been shown to form 1:1 and 1:2 metal complexes with Ag (I) and Cu (II).^{27,28} Other studies have shown that the δ nitrogen of the imidazole ring were bound to Cu(II) in the solid state.²⁹ Attempts were made to complex cHH with Hg (II), but were unsuccessful. Although X-ray quality crystals were not obtained, observed NMR data suggests that the δ nitrogens in the imidazole rings of cHH are primarily responsible for metal coordination.

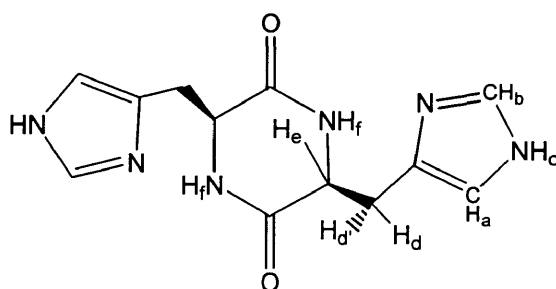


Figure 27: cHH

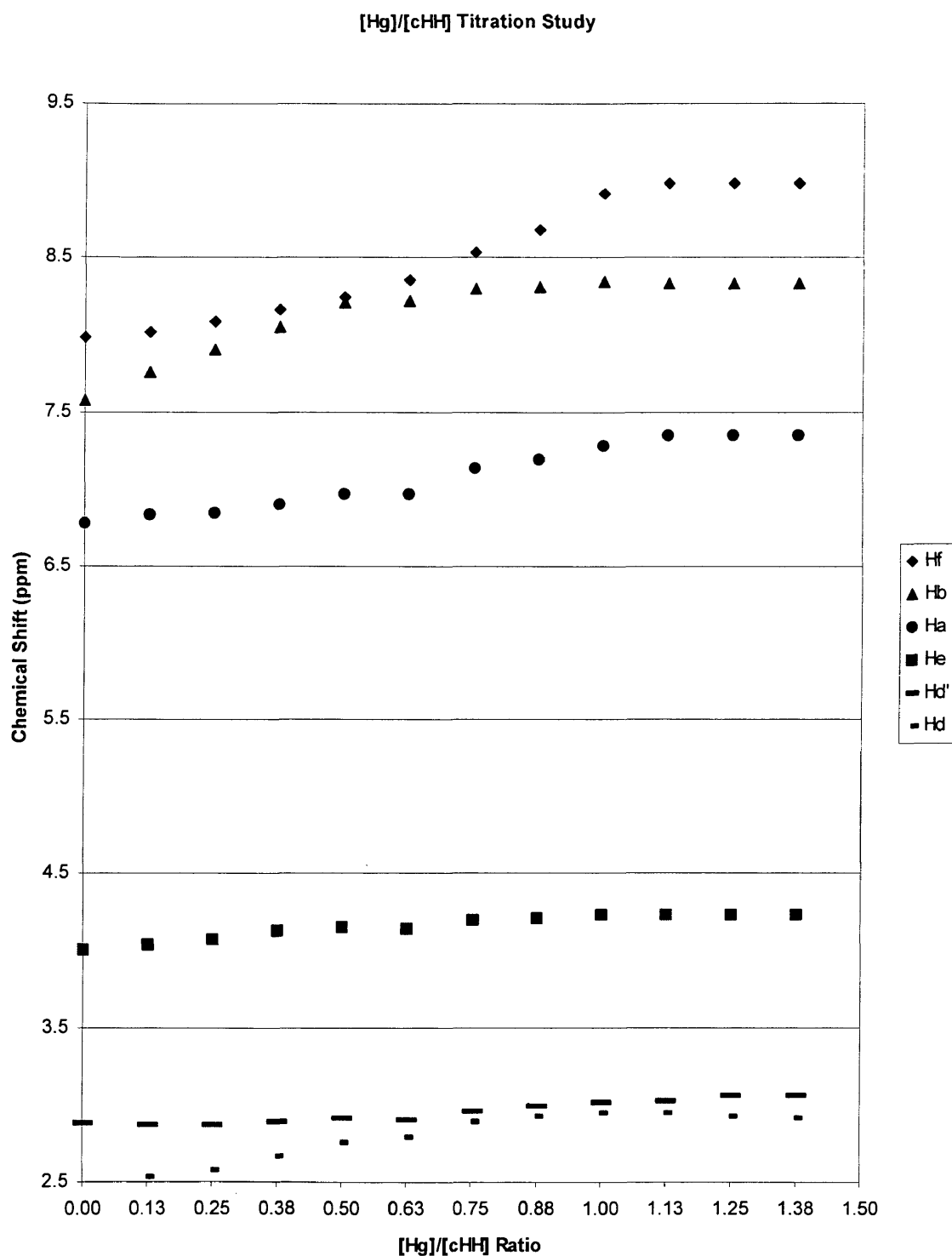


Figure 25: Chemical shifts of protons H_f, H_b, H_a, H_e, H_d', and H_d in cHH in the presence of Hg(ClO₄)₂ as a function of metal-to-ligand ratio in DMSO-d₆ at 20°C are shown. Total metal concentration was 2 mM.

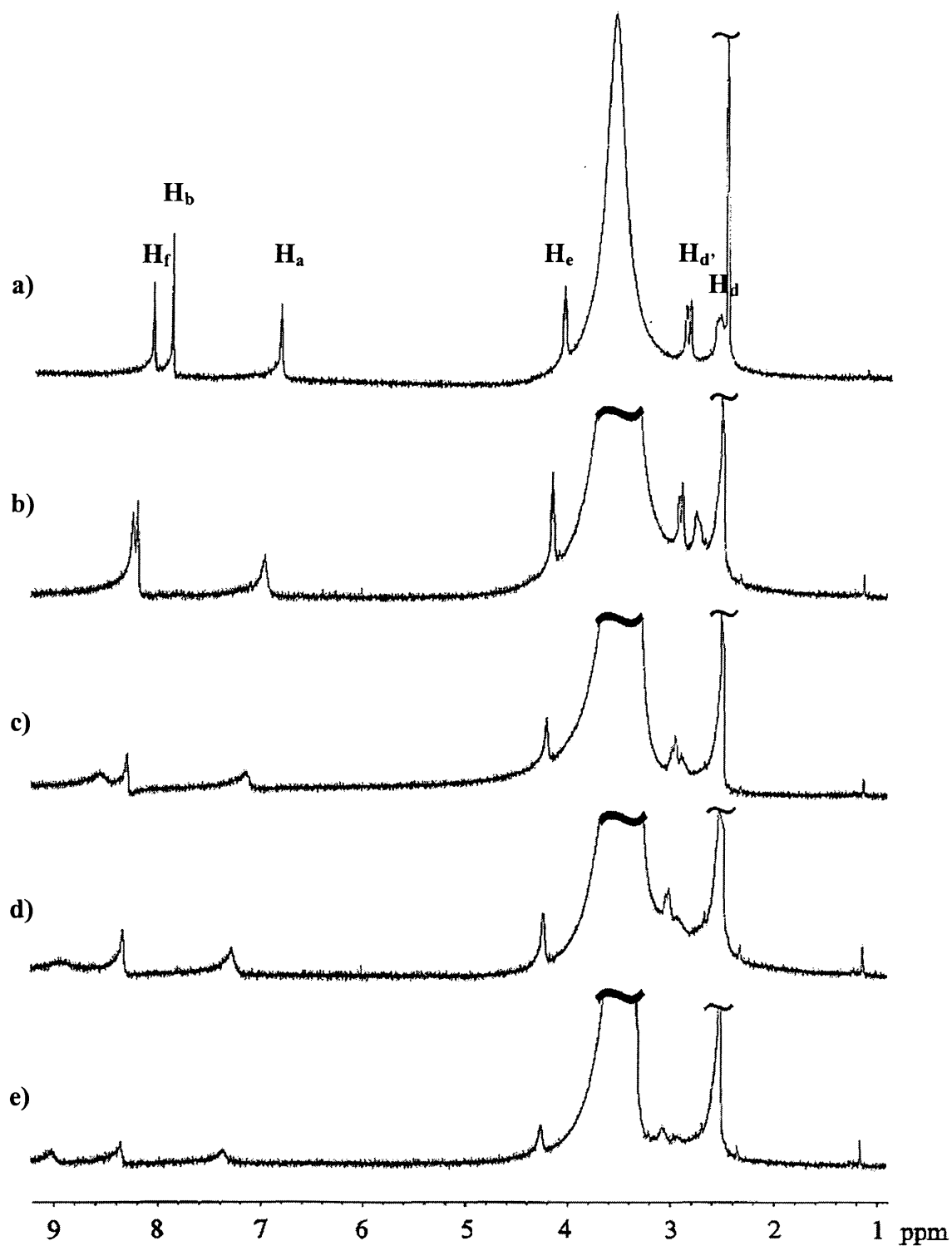


Figure 26: Stack plot of several ^1H NMR spectra of cHH in the presence of $\text{Hg}(\text{ClO}_4)_2$ at 20°C in DMSO-d_6 . Total metal concentration was 2 mM. Metal-to-ligand ratios = a) 0.25, b) 0.50, c) 0.75, d) 1.0, and e) 1.25

The metal-to-ligand ratios of 0.125, 0.25, 0.375, 0.50, 0.625, 0.75, 0.875, 1.0, 1.125, 1.250, and 1.375 were selected to investigate formation of 1:1 and 1:2 complexes. Free cHH was observed to have three relatively sharp peaks between 8.0 and 6.7 ppm. Two of these peaks (H_a and H_b) correspond to the C-H hydrogens on the imidazole ring. The other is the amide proton (H_f) found on the nitrogen next to $C\alpha$ in the cHH ring. This proton shifted the most downfield, moving 1.004 ppm over the course of the study, suggesting the occurrence of changes in the ring structure, like folding.

Each of the C-H imidazole proton resonances (H_b , H_a) were observed to shift significantly downfield (0.746 and 0.572 ppm respective total chemical shifts) over the course of the study. These peaks also broadened significantly compared to those observed in the 1H NMR of free ligand. This is suggestive of an exchange process occurring on a time scale comparable to the NMR time scale or the frequency difference between nuclear environments. H_c was not observed at all in this study. This was expected since proton NMRs of cHH spiked with D_2O and MeOD show this proton is highly exchangeable with both solvents. All of these observations suggest the primary Hg(II) and cHH interaction occurs with the δ nitrogen, as the proton H_b experiences the most significant downfield shift (0.746 ppm) of the two C-H imidazole protons as the Hg:cHH ratio is increased. Also indicative of Hg(II) interaction with the imidazole ring is the shift observed in proton H_d . This proton shifts closer to H_d' from the ratio 0.25 to 1.0 and then appears to move upfield above the 1.0 Hg(II):cHH ratio. This would suggest two things, the first being Hg(II) interaction with the imidazole ring that changes the environment of the H_d and H_d' (methylene) protons by stopping $C\alpha$ -- $C\beta$ bond rotation. Also, since the upfield shift in H_d' resonance stops at the 1.0 ratio, the formation of a 1:1

Hg(II):cHH complex is suggested. The formation of a 1:2 Hg(II):cHH complex may be suggested by the change in the slope of the H_d proton chemical shift plotted in Figure 25. X-ray analysis and further studies will elucidate the exact complex formed.

Overall, this data was highly reproducible. In only one case (proton H_f at 0.375 [Hg]/[cHH]) was the data difference greater than 0.094 ppm. The change observed in chemical shifts of the methylene protons of cHH was similar to the change observed in the chemical shift of the methylene protons of cMM. This similarity between the two studies may further support Hg(II) interaction with the sulfur on the methionyl side chain.

Solution-State Investigations of Cyclo(L-Alanyl-L-Histidyl)

Since alanine is a non-metal binding side chain, cAH was studied with the hopes that titration studies of the dipeptide with Hg(II) would provide better insight into understanding the Hg(II)-histidine interactions observed in the Hg(II):cHH study. A series of solutions in which the Hg:cAH ratio was increased from 0 (free ligand) to 1.375 with 2 mM mercury perchlorate was prepared in DMSO- d_6 . Proton NMR was performed on these solutions at 20°C. Figure 28 shows a plot of chemical shift vs. metal-to-ligand ratio of selected hydrogen atoms. Figure 29 shows a stacked plot of proton NMR spectra at selected metal-to-ligand ratios.

Free cAH (Figure 30) was observed to have four sharp peaks (H_f , H_i , H_b , and H_a) between 6.8 and 8.2 ppm. Each of these peaks were observed to broaden in the presence of Hg(II). This broadening is suggestive of the occurrence of an exchange process. Also of interest was the upfield shift of the amide proton H_f and the C-H imidazole protons H_b and H_a by 0.904, 0.546, and 0.586 ppm, respectively, between free ligand and the 1.375

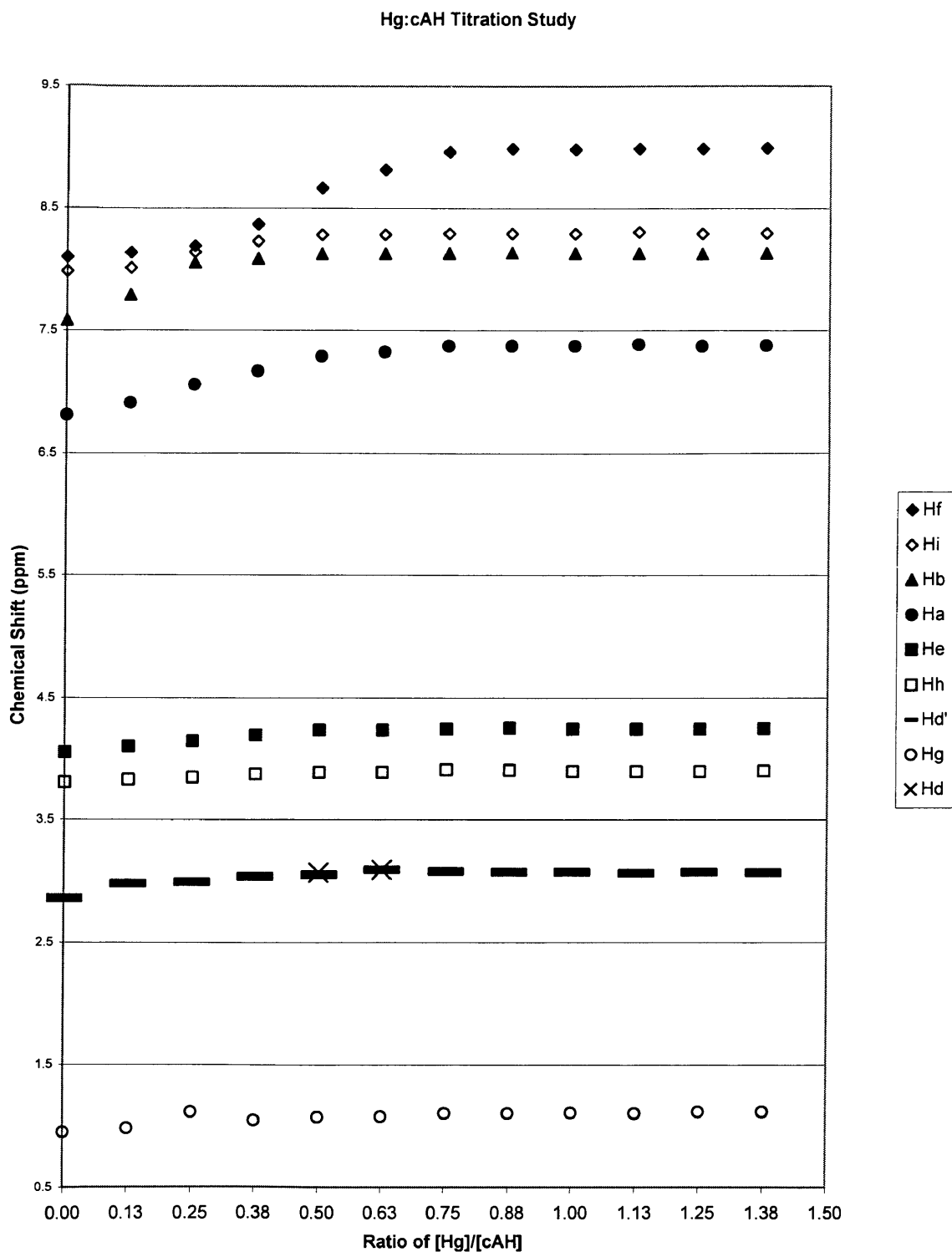


Figure 28: Chemical shifts of protons H_f , H_i , H_b , H_a , H_e , H_h , H_d , and H_g in cAH in the presence of $Hg(ClO_4)_2$ as a function of metal-to-ligand ratio in DMSO- d_6 at 20 °C. Total metal concentration was 2 mM. Histidine protons are represented by solid shapes, while alanine protons are represented by open shapes.

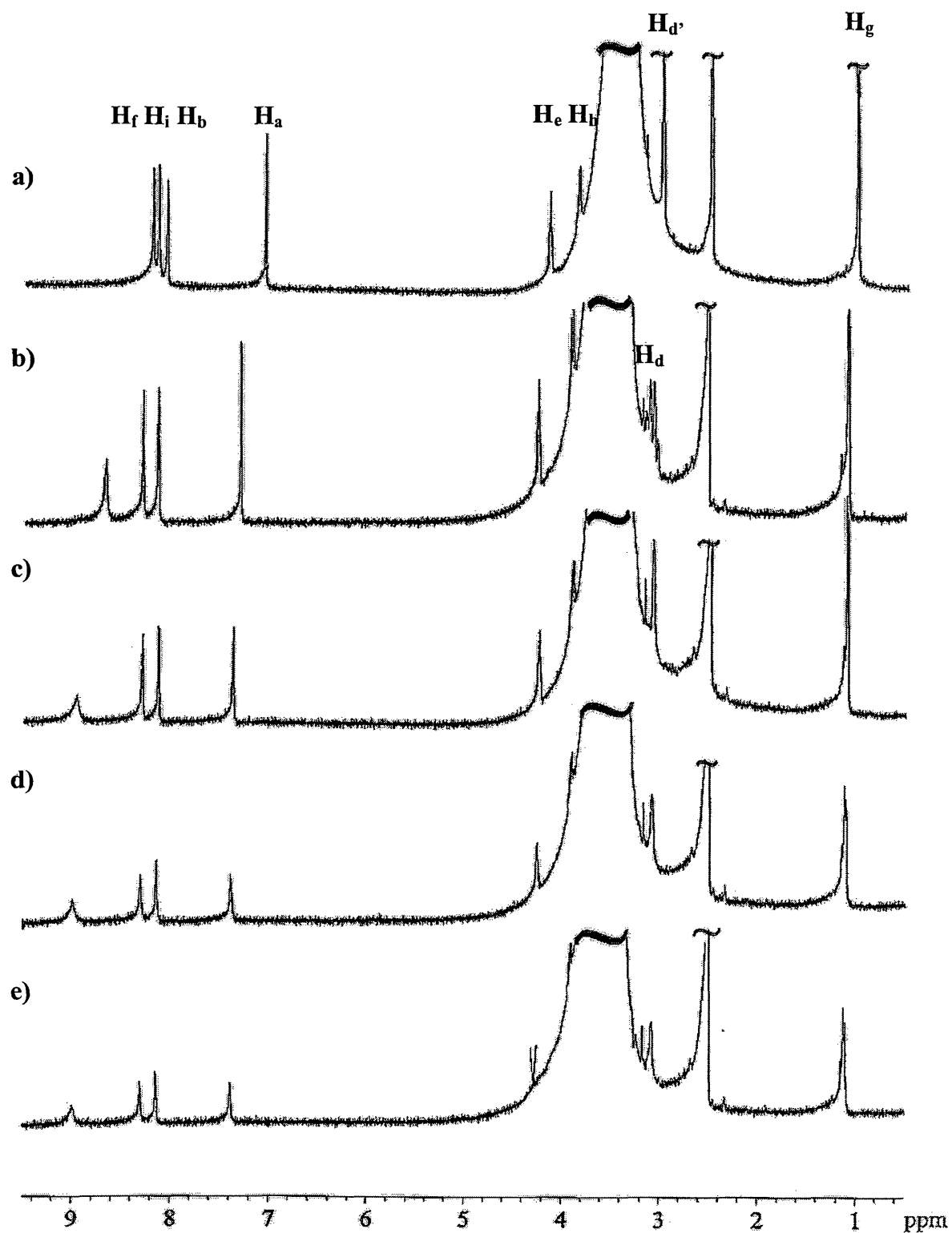


Figure 29: Stack plot of several ^1H NMR spectra of cAH in the presence of $\text{Hg}(\text{ClO}_4)_2$ at 20°C in DMSO-d_6 . Total metal concentration was 2 mM. Metal-to-ligand ratios = a) 0.25, b) 0.50, c) 0.75, d) 1.0, and e) 1.25

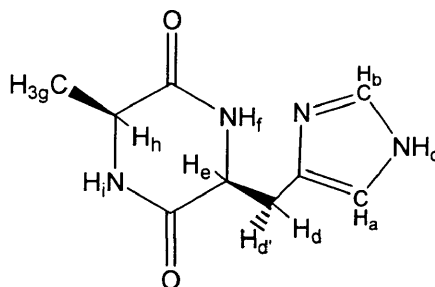


Figure 30: cAH

Hg(II):cAH ratio. A change in the H_b and H_a proton environments suggested by the change in the chemical shift of these protons may also indicate the formation of a Hg(II)-cAH complex. H_b shifts the greatest over the course of the study, which supports the interaction of mercury (II) with the δ nitrogen on the imidazole ring. Since H_b is the closest proton of the imidazole ring to the proposed mercury interaction site, one would expect to note the greatest change the chemical shift of this proton. Another point of interest is the upfield shift of H_f which suggests a change in the cAH ring environment consistent with the formation of a Hg(II)-cAH complex. The change in the slope of the protons H_f, H_a, and H_b (plotted in Figure 27) seems to level off at ratios of Hg(II):cAH above 0.5. This may suggest the possible formation of a 1:2 Hg(II):cAH complex. Also, the change observed in H_d between 0.25 and 0.5 from a singlet to an overlapping doublet of doublets indicates a change in the stereochemistry of the methylene protons, which may support this possibility of 1:2 complex formation. The doublet of doublets reverts to a singlet at ratios above 0.625, which is why only two H_d' points (represented by an x) are plotted in Figure 28. H_d also broadens in the presence of Hg(II), suggesting the occurrence of an exchange process, which further suggests the formation of a Hg(II):cAH

complex. This interpretation of results is only cursory, requiring further NMR and X-ray analysis studies for confirmation.

The alanyl protons H_g , H_h , and H_i remained nearly unchanged throughout the study, shifting at total of 0.166 ppm, 0.094 ppm, and 0.311 ppm, respectively, over the course of the study. This indicates that the environment of the alanyl protons changes minimally over the course of the study. Therefore, the association between mercury (II) and cAH most likely occurs on the histidyl side chain since the greatest change in chemical shift is observed with the histidyl protons, which supports the observations and analysis of the Hg(II):cHH titration study.

IV. NMR SOLUTION-STATE STUDIES OF CADMIUM(II) COORDINATION

Solution-State Investigations of Cyclo(L-Histidyl-L-Histidyl)

A series of solutions in which the Cd:cHH ratio was increased from 0 (free ligand) to 3:2 with 2 mM cadmium perchlorate was prepared in DMSO-d₆. Proton NMR was performed on these solutions at room temperature. Figure 31 shows a plot of chemical shift vs. metal-to-ligand ratio of selected hydrogen atoms. Figure 32 shows a stacked plot of proton NMR spectra at selected metal-to-ligand ratios.

In general, peak broadening, suggestive of exchange processes occurring, is apparent in all cadmium containing samples, when compared to the ¹H NMR spectra of free cHH (Appendix 5). The presence of free ligand is apparent throughout the study, as indicated by constant slope of the solid shapes in Figure 31. The intensity of the free ligand peaks noticeably decreases over the course of the study, suggesting a decrease in overall free ligand. Additional peaks at 8.19, 7.43, 6.04, and 4.31 ppm arise at the 0.375 and 0.50 ratios of Cd:cHH and increase in intensity over the course of the study suggesting that a Cd:cHH complex is forming. Since two sets of cHH resonances were not observed in identical Hg:cHH studies, cadmium may exchange more slowly than mercury under these study conditions. Analysis of the behavior of the H_d and H_{d'} protons was complicated by potential overlap with the broad water and DMSO-d₆ resonances. However, it appears the peaks of H_d and H_{d'} migrate to overlap at 2.83 ppm. The overlap of the two protons begins at the 1.0 ratio of Cd(II):cHH and continues throughout the rest of the study. This trend suggests the formation of a 1:2 Cd(II):cHH complex.

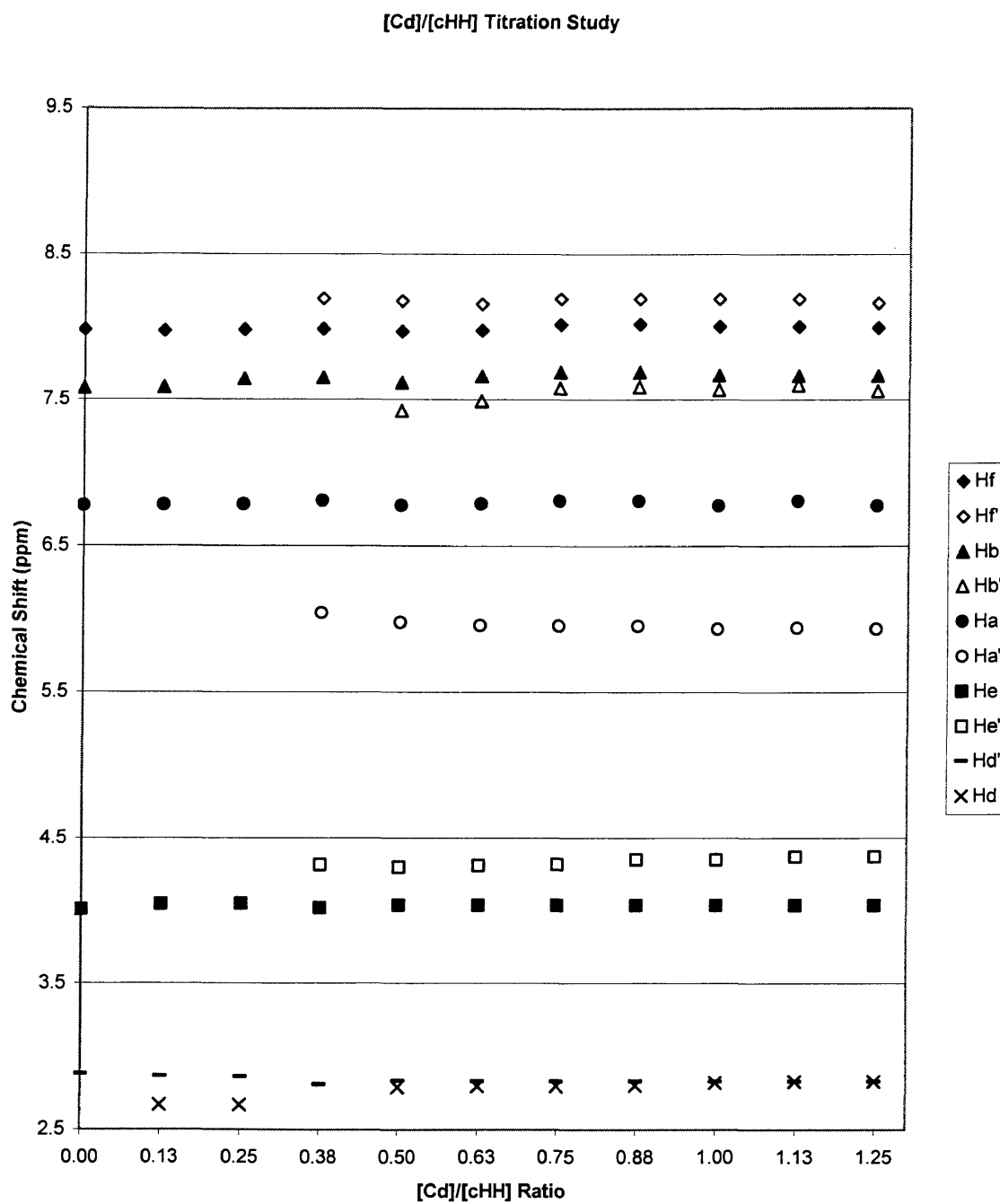


Figure 31: Chemical shifts of protons H_f, H_b, H_a, H_e, and H_d in cHH in the presence of Cd(ClO₄)₂·H₂O as a function of metal-to-ligand ratio in DMSO-d₆ at room temperature. Total metal concentration was 2 mM.

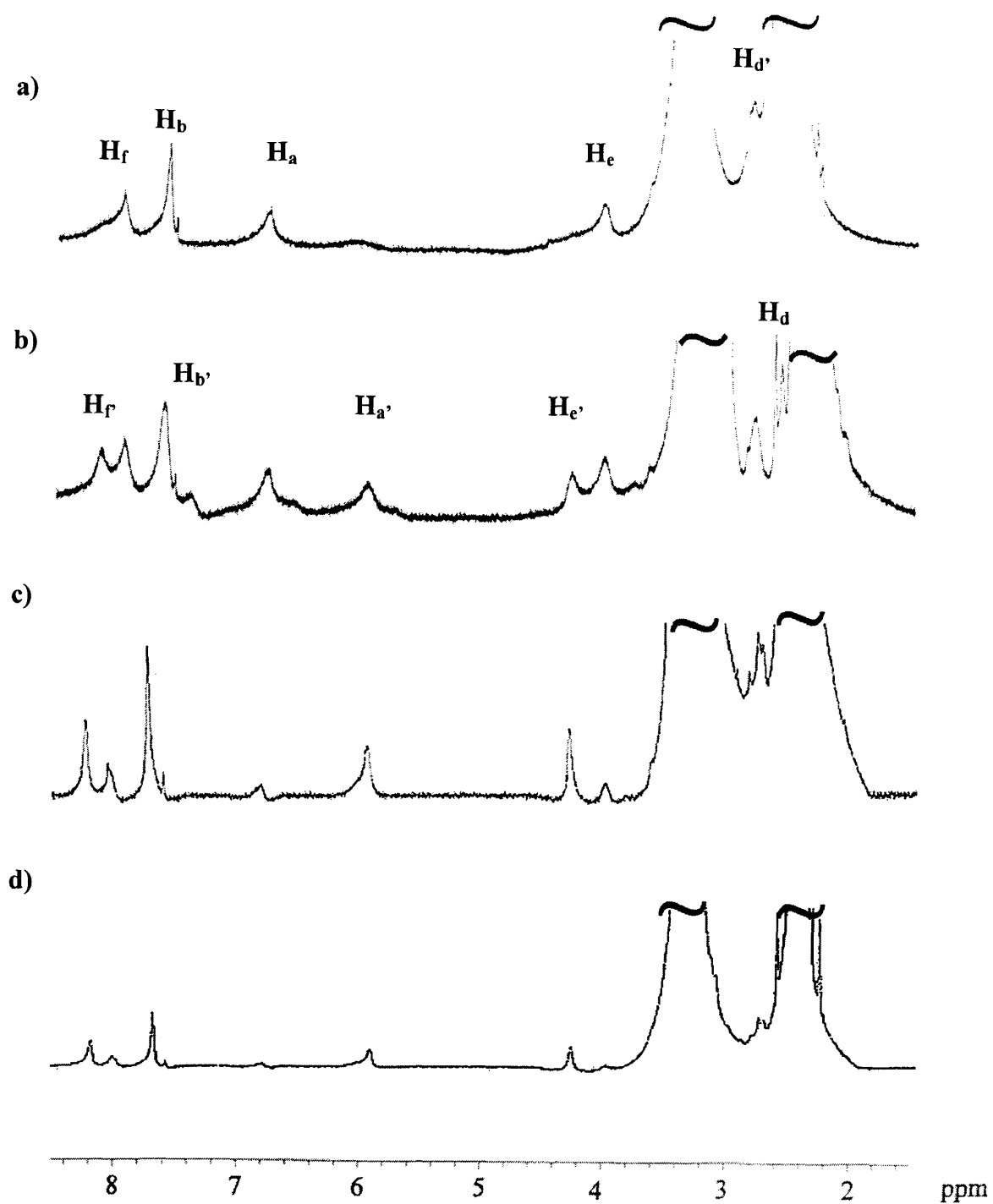


Figure 32: Stack plot of several ^1H NMR spectra of cHH in the presence of $\text{Cd}(\text{ClO}_4)_2 \cdot \text{H}_2\text{O}$ at 20°C in DMSO-d_6 . Total metal concentration was 2 mM. Metal-to-ligand ratios = a) 0.25, b) 0.50, c) 0.75, and d) 1.0

Recent studies have shown that both cadmium (II) and mercury (II) can be substituted for and readily adopt the coordination environment of native metal ions.^{10, 30-34} Comparable binding of Cd(II) and Hg(II) to small ligands has also been observed.³⁵ ¹H NMR studies with small, non-oxygen containing ligands have suggested that the solution equilibria of the Cd(II) and Hg(II) systems were comparable as the proton chemical shifts with various mole ratios of Cd(II) were only shifted slightly downfield in comparison to identical ratios of Hg(II).³⁵ In the Cd:cHH titration study, the ligand-metal complex proton shifts are significantly different from the trend observed in the Hg:cHH study.

In general, cHH proton chemical shifts increase in the presence of Hg(II), whereas in the cadmium study no general trend of proton shifting can be assessed. The Cd(II) complex related protons H_e' and H_f' shift slightly downfield from free ligand (0.3 and 0.2 ppm, respectively), while H_b' shifted slightly upfield (0.2 ppm) and H_a' shifted significantly upfield (0.8 ppm). This appreciable difference in trends between cadmium and mercury titration studies may be attributable to the presence of oxygen in the cHH ligand used. This is supported by previous indications that cadmium (II) and mercury (II), while in the same periodic family, possess complementary coordination preferences.³⁵ Cadmium preferentially binds to hard ligands like oxygen, while softer ligands, like sulfur, are preferred by mercury.³⁵ Since cadmium is more oxophilic, there is a possibility of different binding modes with oxygen containing ligands, which may explain the difference between the observed Hg(II) and Cd(II) complexing trends with cHH.

CONCLUSION

The syntheses of cyclo-(L-alanyl-L-methionyl) was completed by using a strategy that employed protecting the nitrogen terminus with N-benzyloxycarbonyloxy and protecting the carboxy terminus with a methyl ester to prevent multimerization and racemization. The syntheses of cyclo-(L-alanyl-L-histidyl) and cyclo(L-leucyl-L-prolyl) were completed using similar strategies. Integration of cLP into β CD was unsuccessful because cLP did not associated with β CD as predicted. This may be a result of the β CD cavity being either too small or too large. Future studies should be aimed at attempting cLP integration into either α or γ CD, which have different cavity sizes.

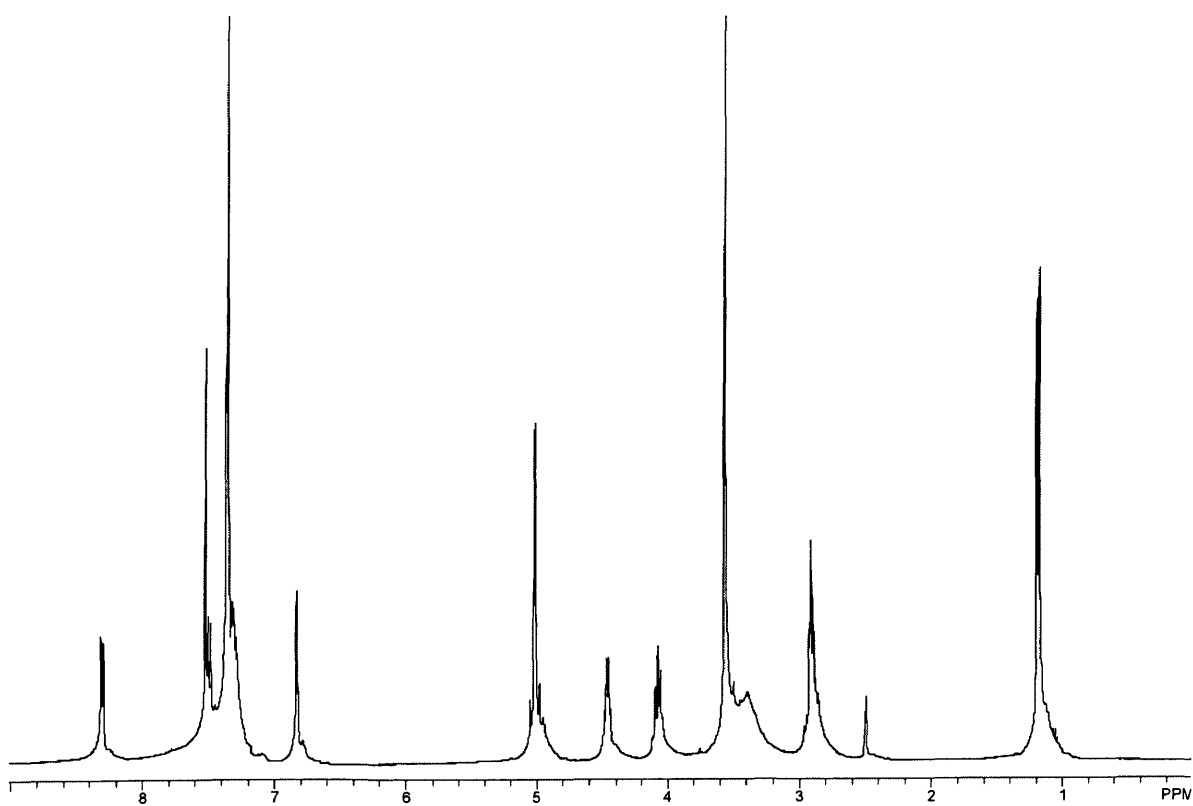
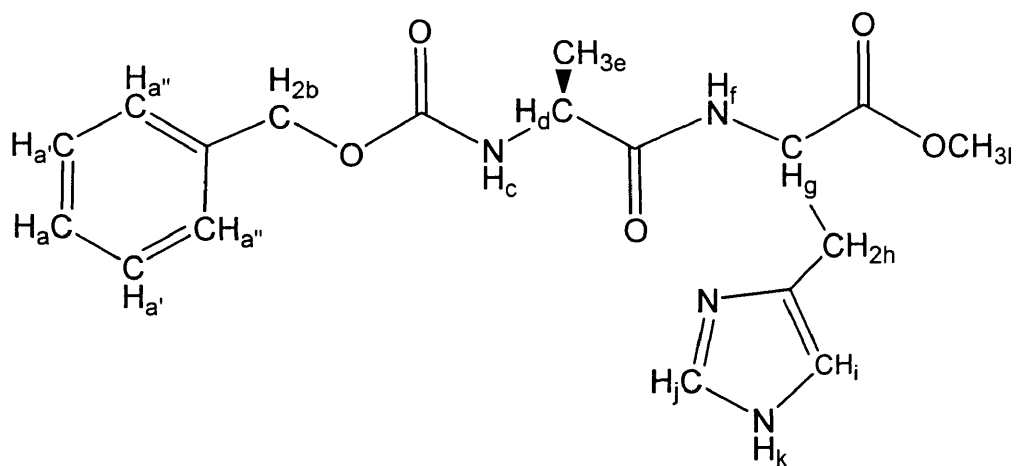
The analysis of cMM NMR titration data in DMSO- d_6 proved to be more difficult than expected. The coordination of Hg(II) and methionyl is remotely suggested by both the cMM and cAM titration studies, which also indicate the possibility of 1:2 and 1:1 complex formation. However, further evaluation of these interactions is needed to substantiate these rudimentary conclusions.

The histidyl side chain, specifically the δ nitrogen of the imidazole ring, was tentatively established as the primary site for Hg(II) interaction in cAH and cHH. Analysis indicates that there is an intermediate exchange rate in the equilibrium that is too slow on the NMR time scale for a sharp, time averaged signal. In the presence of mercury, there is evidence that the exchange rate is too fast for individual species detection. Analysis of the Cd(II) titration study provides some evidence that the

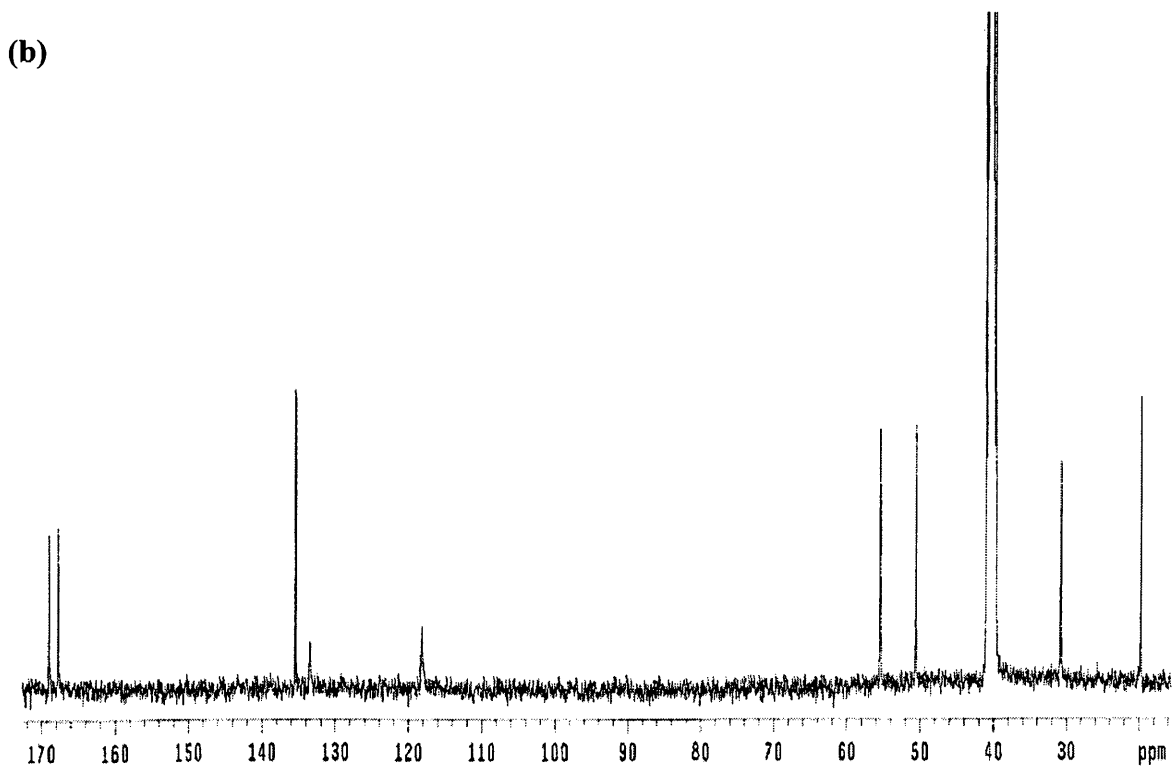
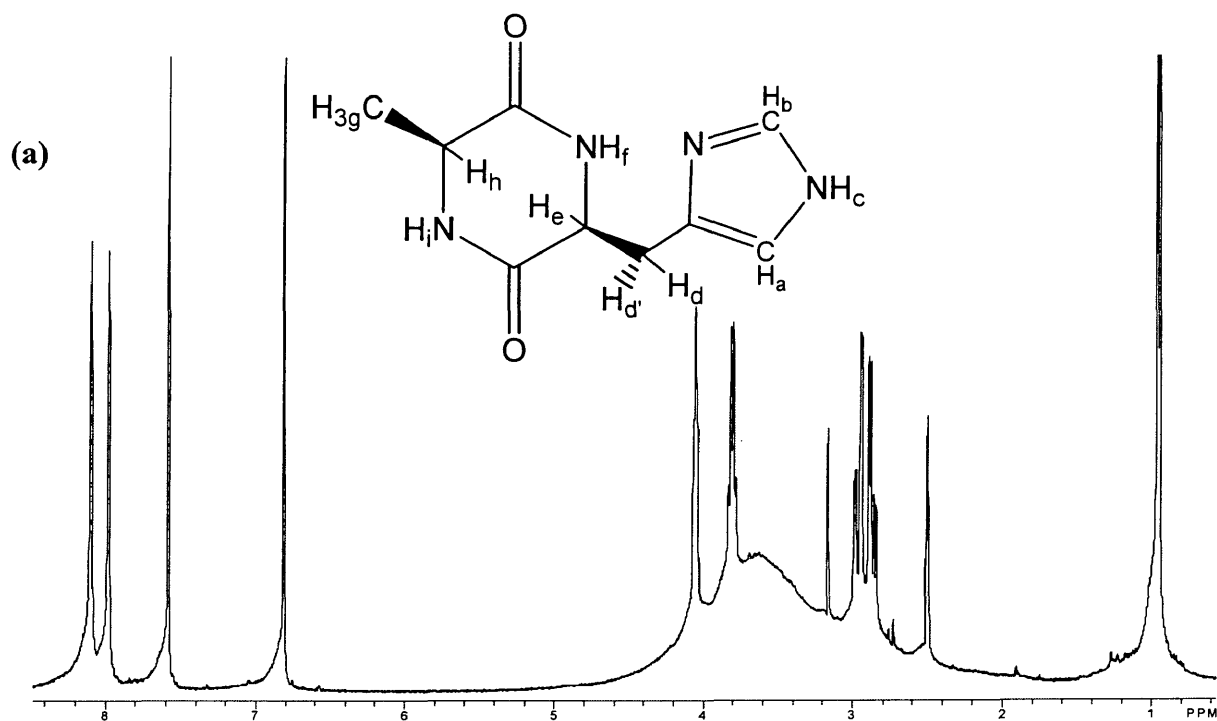
exchange process in the presence of cadmium is slower than that observed in the mercury study, as multiple species peaks are distinct. These conclusions are however merely speculative, as X-ray analysis of solid crystals corresponding to these complexes has not been achieved.

The low solubility of cHH and its complexes in solution has proven the greatest problem in growing the crystals needed for X-ray analysis. While solvents have been discovered to solvate Hg(II):cHH complexes, they possess high boiling points and are not favorable for slow evaporation crystal growing. Alternate strategies, like cosolvent layering, have not been successful at this time, as a cosolvent that is miscible with DMSO in all proportions that does not solvate cHH or its complexes has not been identified.

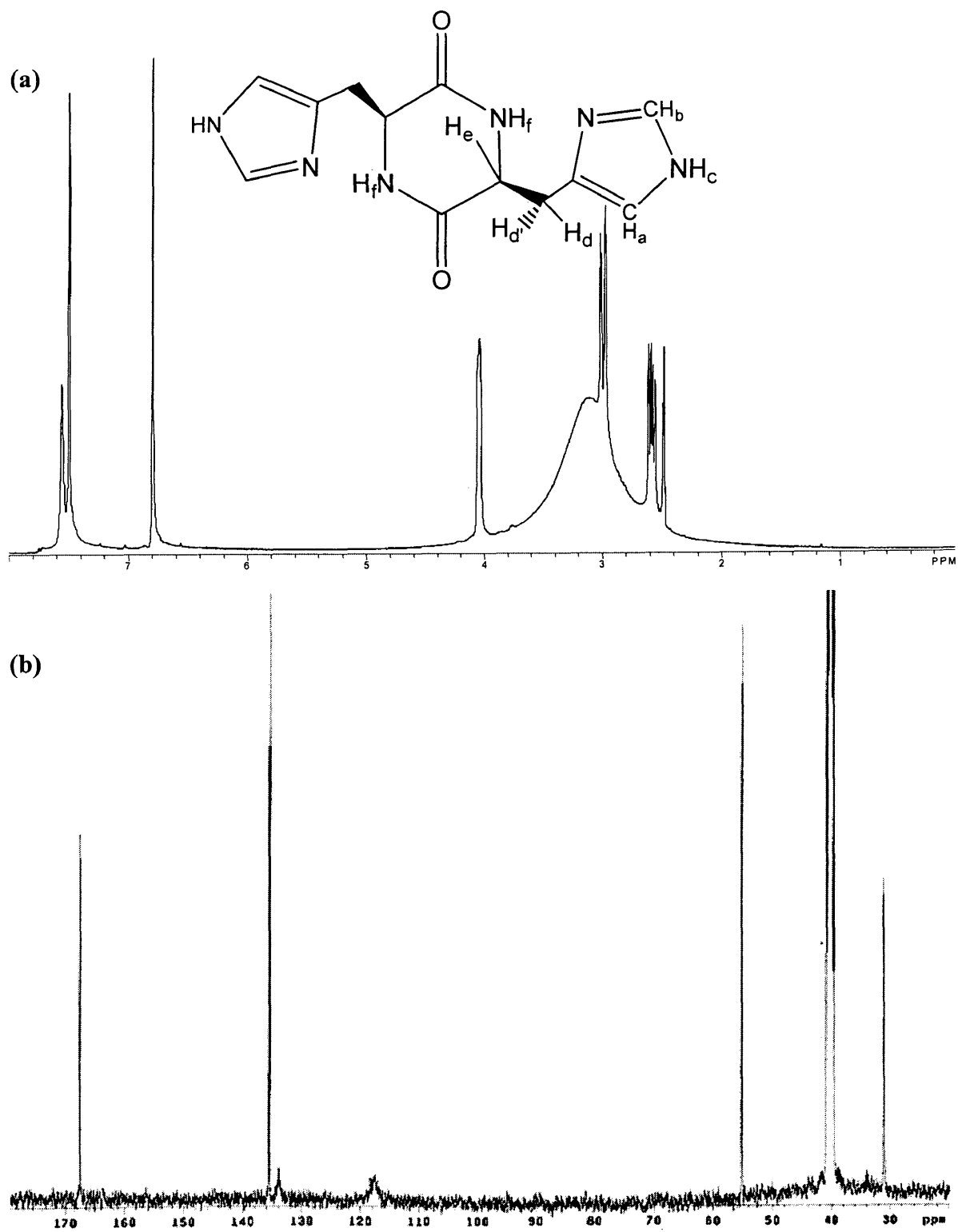
Immediate future plans include synthesis and X-ray analysis of Hg:cHH crystals obtained in 1:1 and 1:2 metal-to-ligand ratios, as well as X-ray analysis of α or γ cyclodextrin integrated cLP crystals made in 1:2 ratio of guest to host. Pending are solid-state NMR analyses of labeled and unlabeled cLP as a free ligand and as a guest in either α or γ cyclodextrin in 1:2 guest to host ratio. Also incomplete at this time are mass spectrometry studies on cLP, LPOMe, PLOMe and PPOMe. Overall, this study was designed to provide a library of characterizations of the synthesized dipeptides to be compared with results of the eventual investigation of the potential of ^{199}Hg NMR to structurally characterize metalloproteins. Future research in this laboratory is aimed at exploring the utility of mercury NMR in the characterization of structural features of protein metal coordination sites.



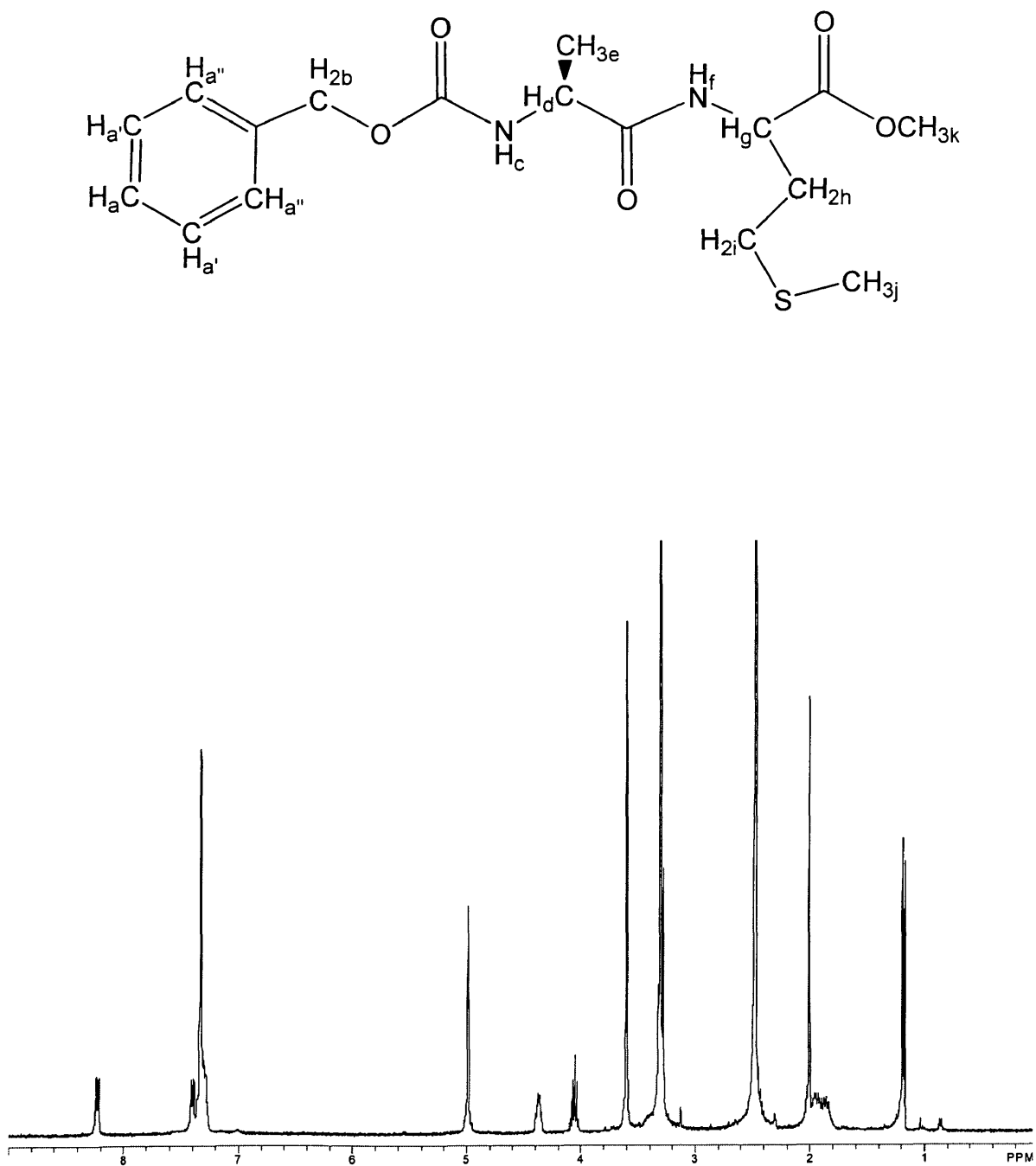
Appendix 1: ^1H NMR of 166 mM ZAHOMe in DMSO-d_6 at 20°C .



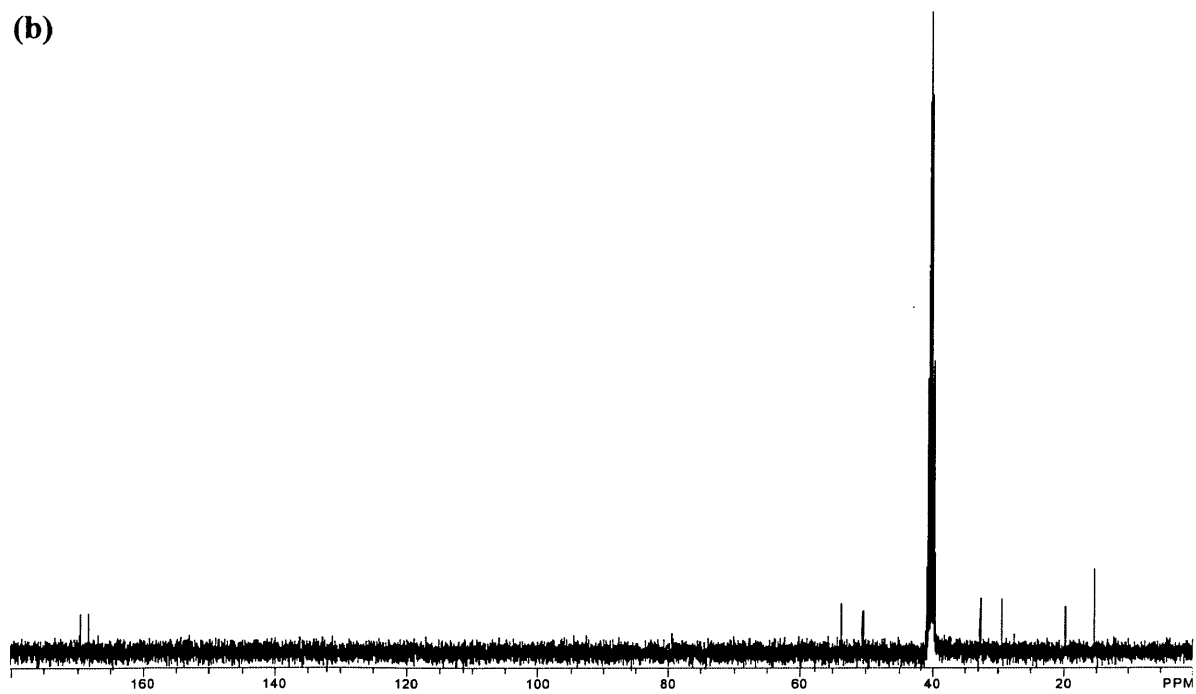
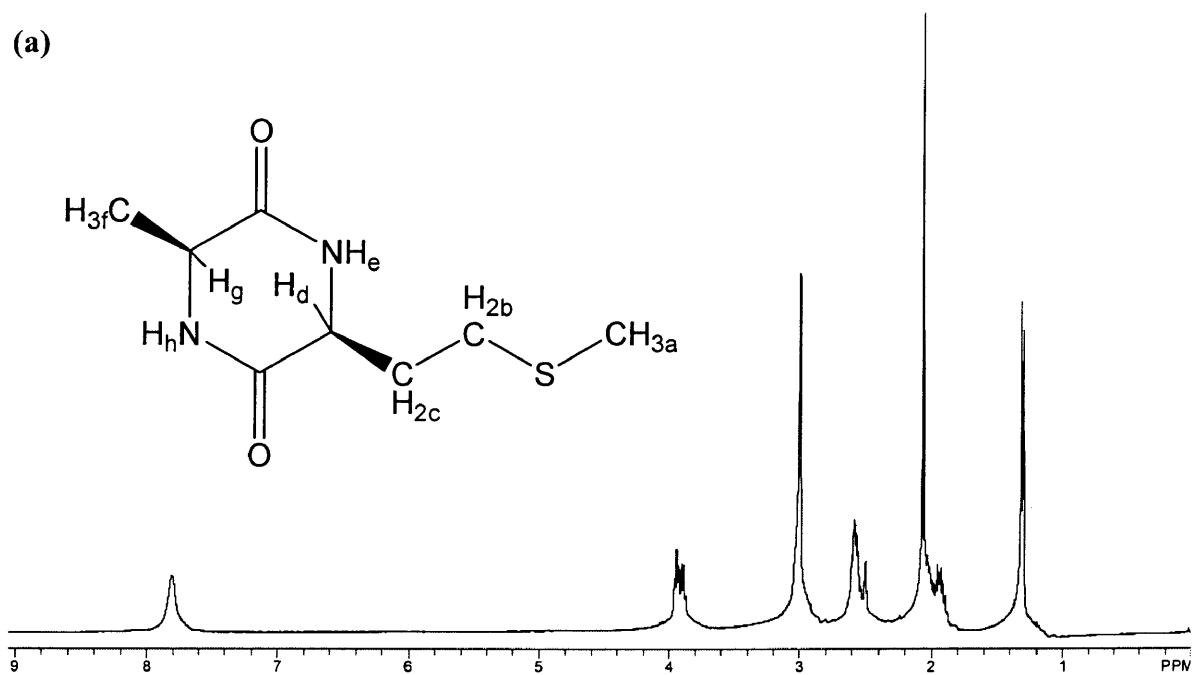
Appendix 2: (a) 1H NMR of 235 mM cAH in DMSO- d_6 at 20°C. (b) ^{13}C NMR of 235 mM cAH in DMSO- d_6 at 20°C.



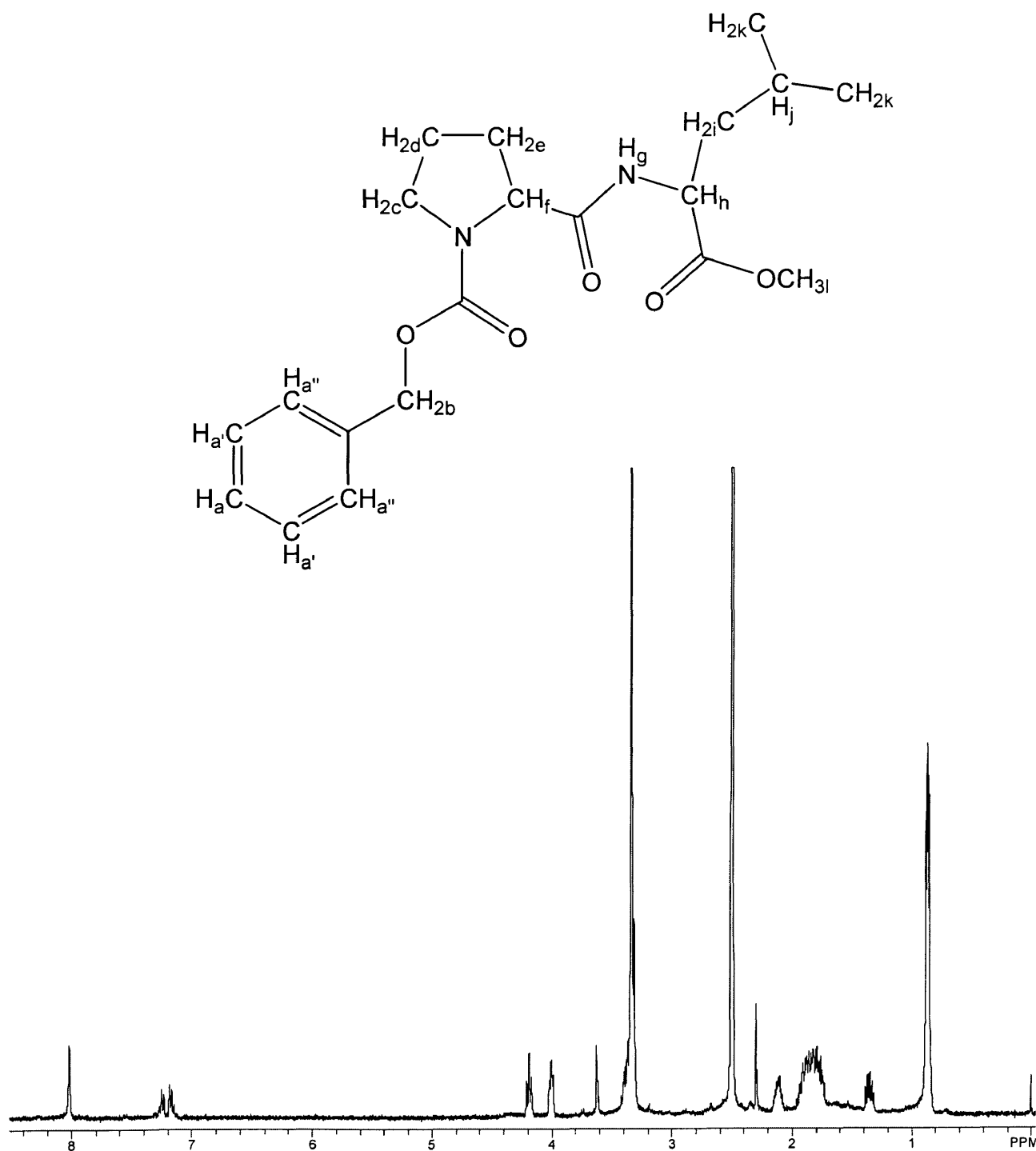
Appendix 3: (a) ^1H NMR of 68 mM cHH in DMSO-d_6 at 100°C . (b) ^{13}C NMR of 68 mM cHH in DMSO-d_6 at 20°C .



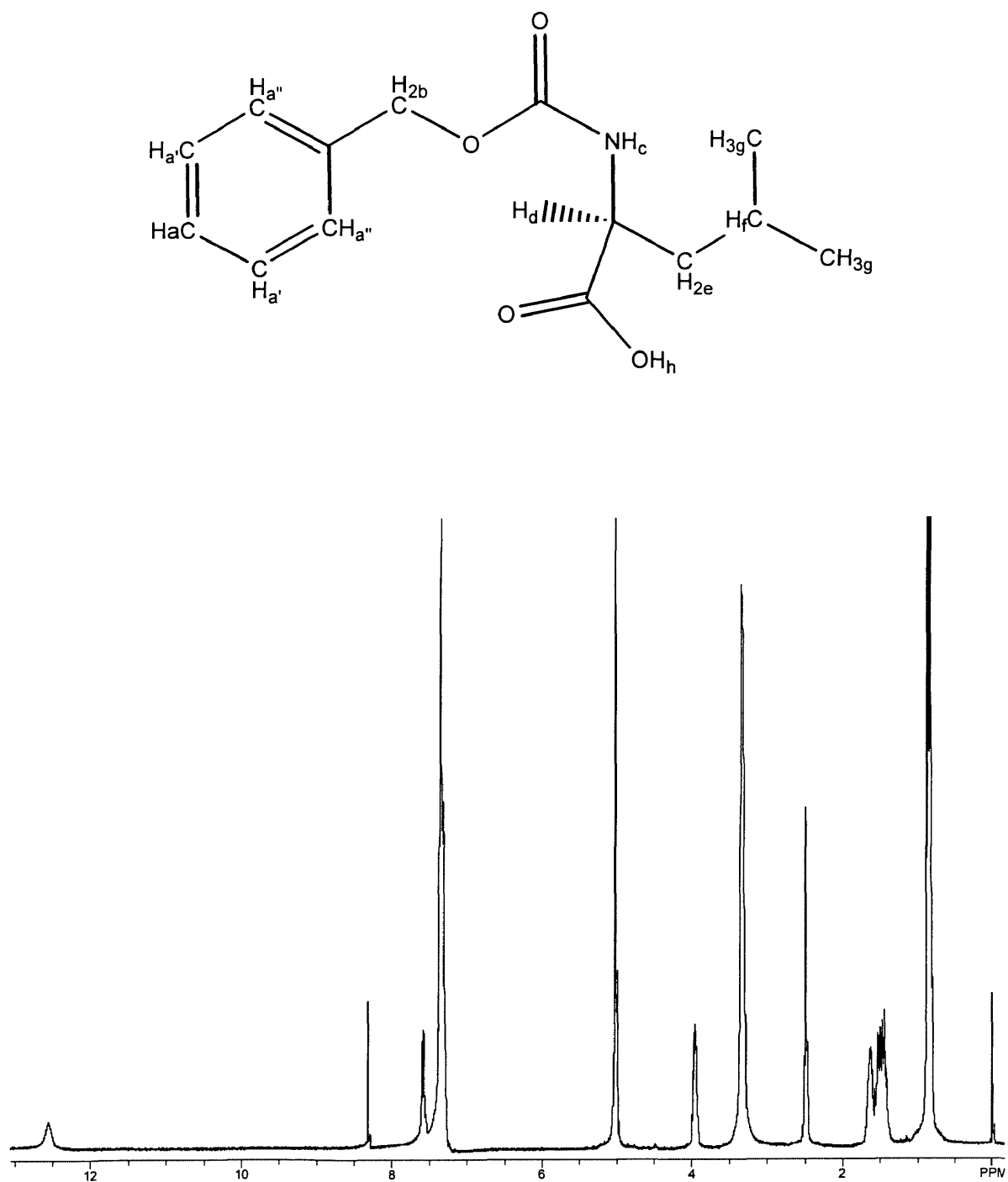
Appendix 4: ^1H NMR of ZAMOMe at room temperature in DMSO-d_6 . Concentration unknown.



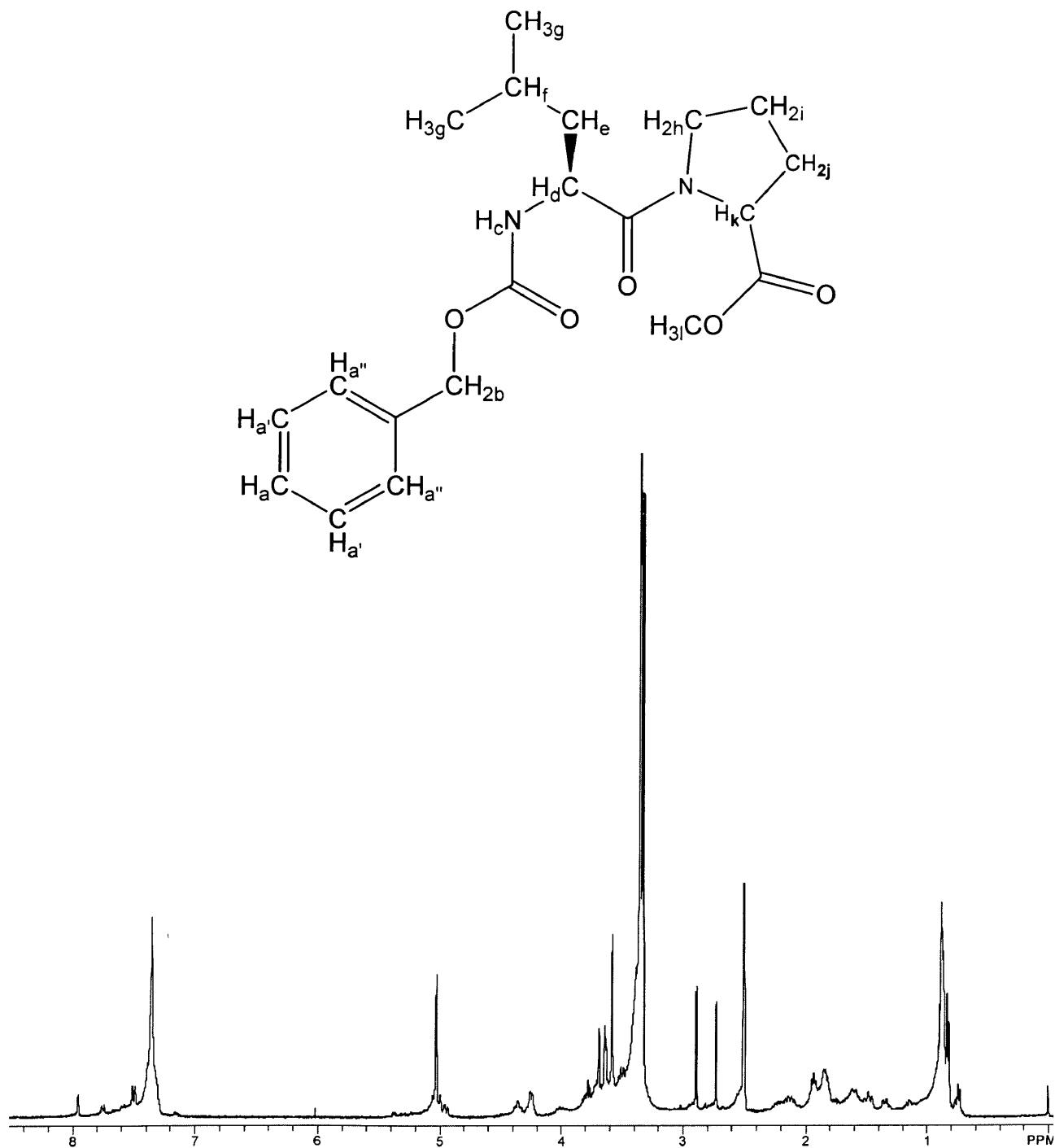
Appendix 5: (a) ^1H NMR of 118 mM cAM in DMSO- d_6 at 100°C. (b) ^{13}C NMR of 118 mM cAM in DMSO- d_6 at 20°C.



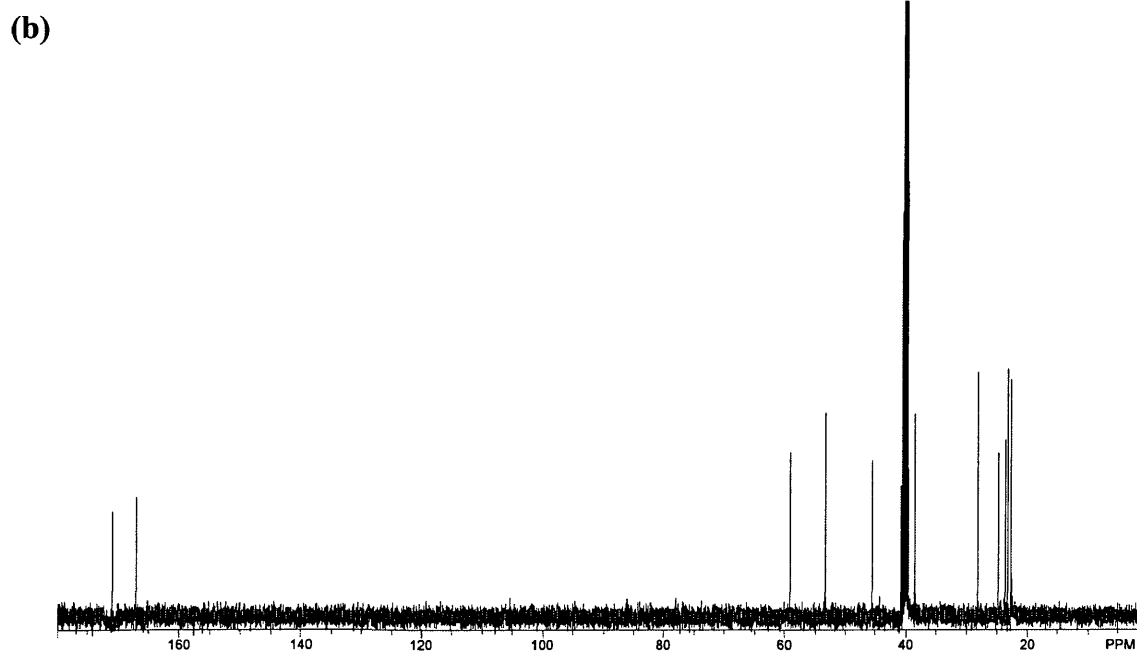
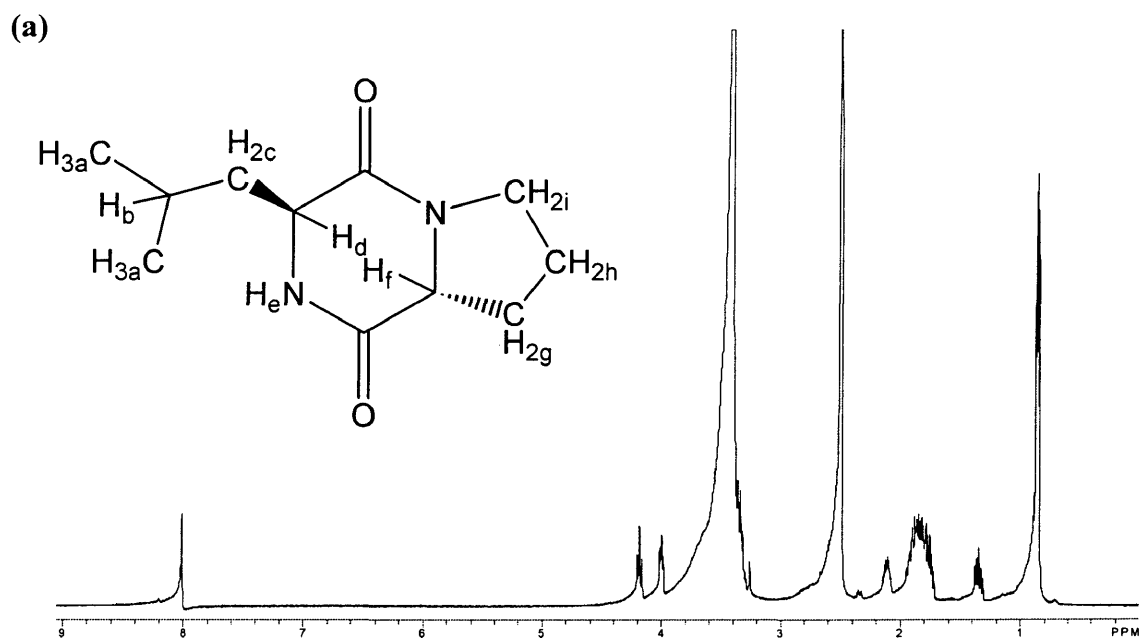
Appendix 6: ^1H NMR of ZPLOMe in DMSO-d_6 at 20°C . Concentration unknown secondary to ZPLOMe being an oil.



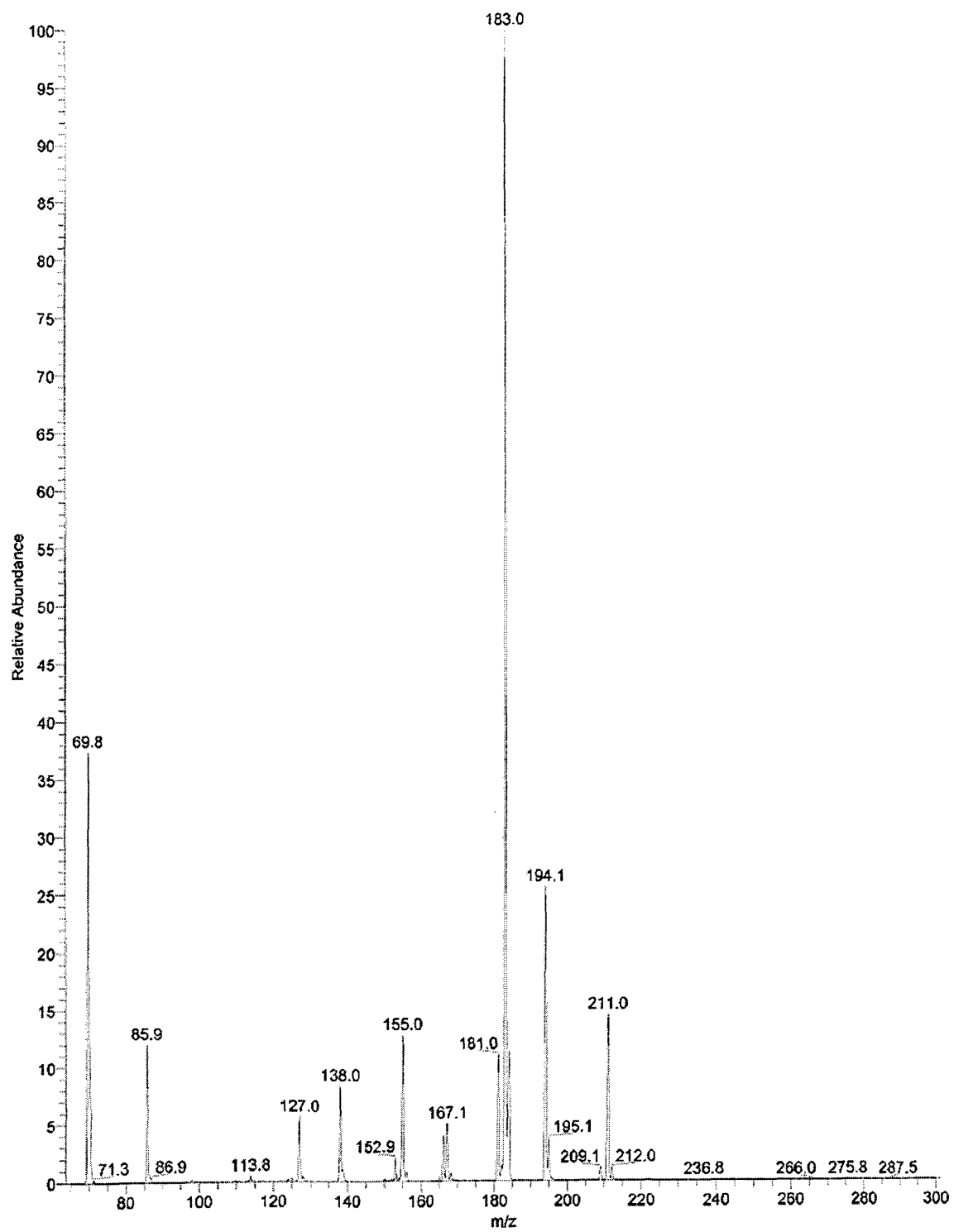
Appendix 7: ^1H NMR of Z-LeuOH in DMSO- d_6 at 20°C. Concentration of sample unknown secondary to Z-LeuOH being an oil.



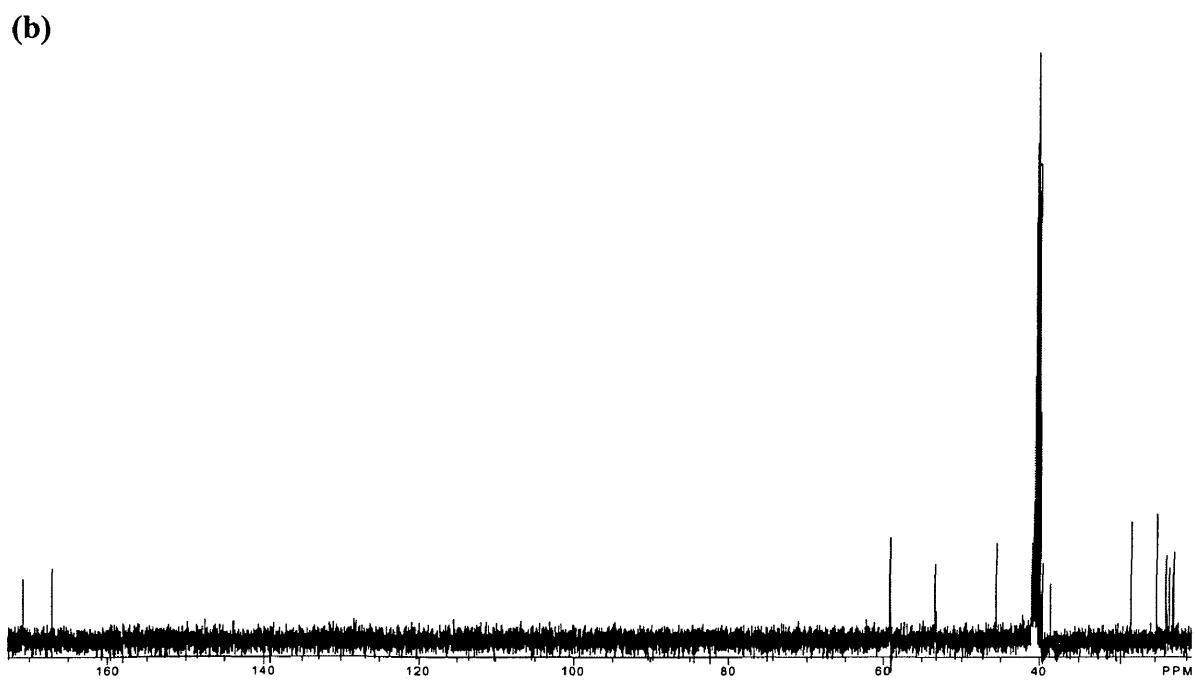
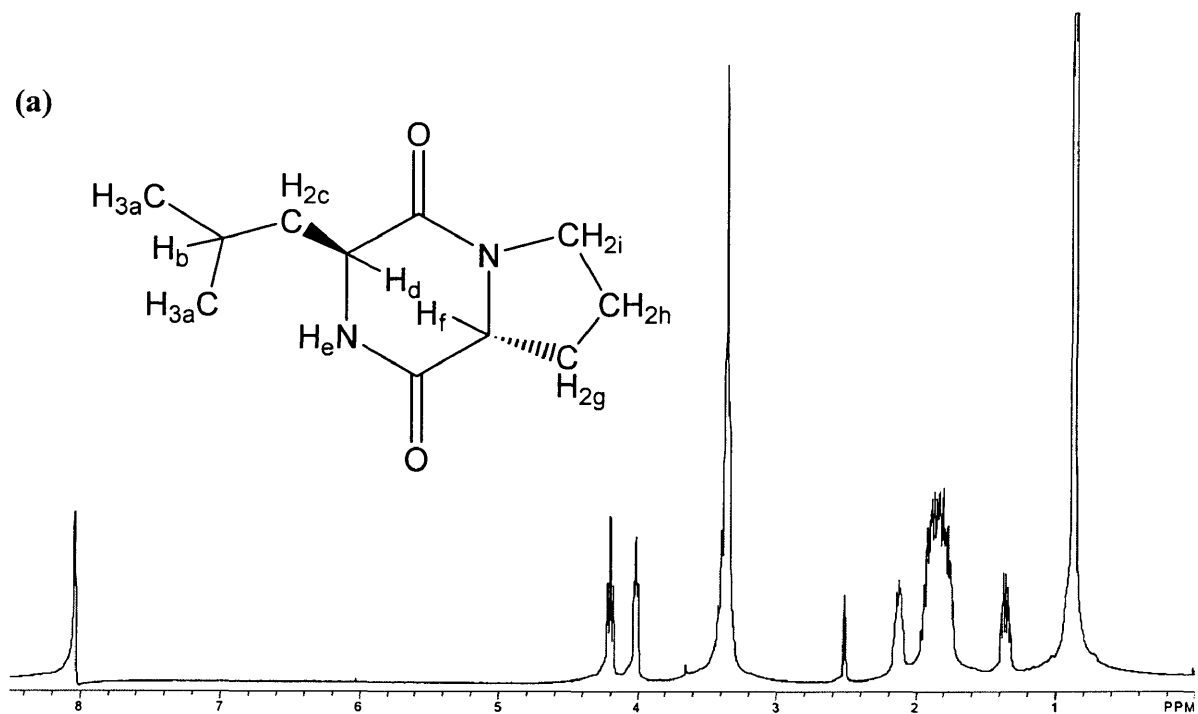
Appendix 8: ^1H NMR of ZLPOMe in DMSO-d_6 at 20°C . Concentration of sample unknown secondary to ZLPOMe being an oil.



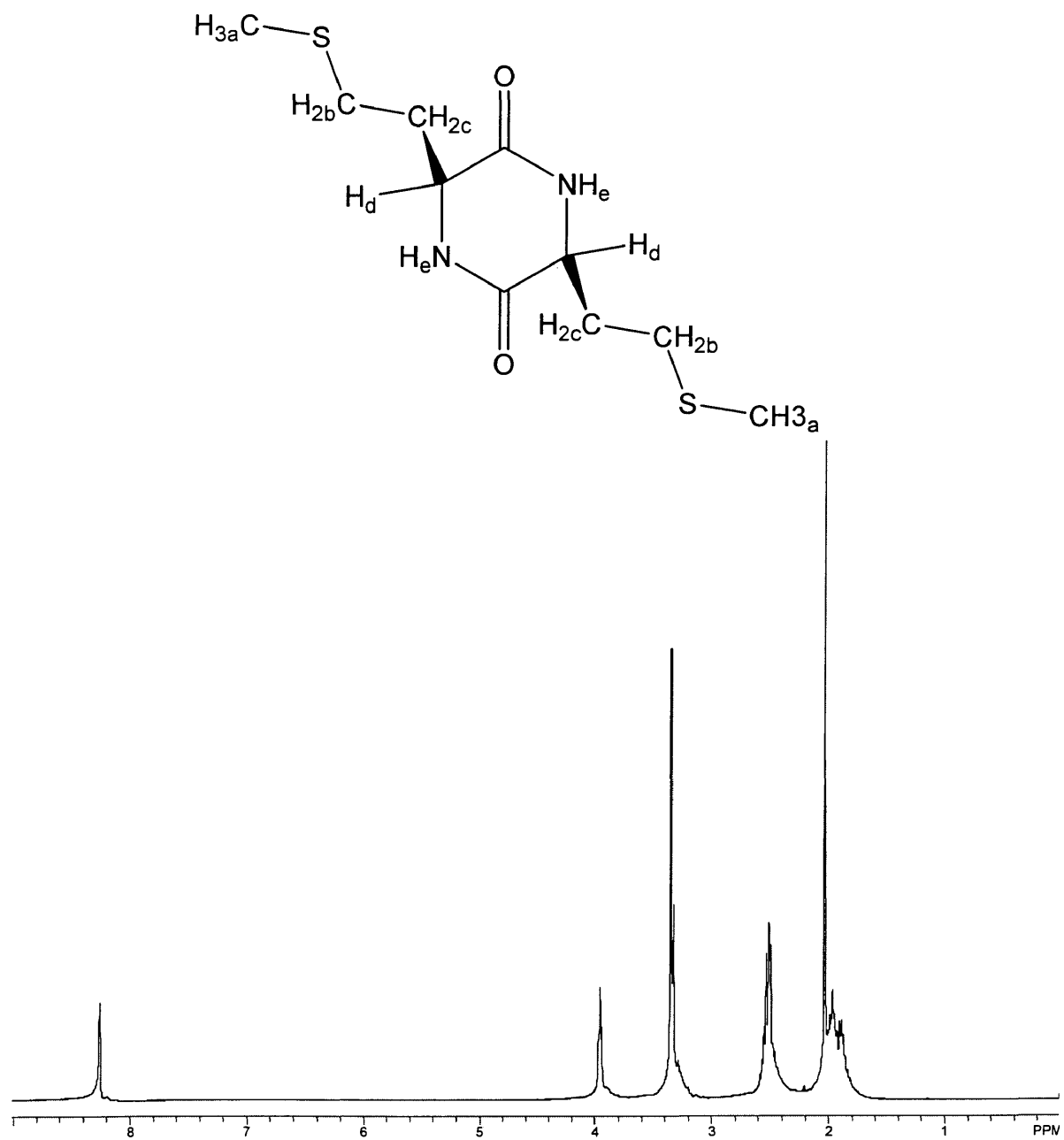
Appendix 9: (a) ¹H NMR of 140 mM cLP in DMSO-d₆ at 20°C. (b) ¹³C NMR of 140 mM cLP in DMSO-d₆ at 20°C.



Appendix 9: c) Mass Spectrometry of cLP in H₂O:CH₃OH (50:50 v/v).



Appendix 10: (a) 1H NMR of 141 mM cPL in DMSO- d_6 at 20°C. (b) ^{13}C NMR of 141 mM cPL in DMSO- d_6 at 20°C.



Appendix 11: ^1H NMR of 55 mM cMM in DMSO- d_6 at 20°C.

REFERENCES

1. Anfinsen, C., Haber, E., Sela, M. White, F. *Proc. Natl. Sci. USA*, **1961**, *47*, 1309-1314.
2. Thomas, P., Q, B., Pedersen, P. *Trends in Biochemical Sciences*. **1995**, *20*, 456-459.
3. Strobel, H., Heineman, W. *Chemical Instrumentation: A Systematic Approach*, 3rd Ed., John Wiley & Sons, Inc.: New York, **1989**.
4. Pine, S., Hendrickson, J., Cram, D., Hammond, G. *Organic Chemistry*. McGraw-Hill Book Company.: New York, **1980**, 132.
5. Johnstone, R., Rose, M. *Mass Spectrometry for Chemists and Biochemists*, 2nd Ed., Cambridge University Press.: New York, **1996**.
6. Vollhardt, K., Schore, N. *Organic Chemistry*. W.H. Freeman and Company, **1994**, 328-331.
7. Homans, S. *A Dictionary of Concepts in NMR*, Clarendon Press: Oxford, **1989**.
8. Silverstein, R., Webster, F. *Spectrometric Identification of Organic Compounds*, 6th Ed., John Wiley & Sons, Inc.: New York, **1998**.
9. Borman, S. *C & E News*. **2001**, 40-41.
10. Utschig, L., Bryson, J., O'Halloran, T. *Science*. **1995**, *268*, 380-385.
11. Church, B., Guss, M., Potter, M., Freeman, H., *J. Biol. Chem.*, **1986**, *261*, 234-237.
12. McKee, J., McKee, T. *Biochemistry*. McGraw-Hill: New York, **1999**, 363-377.
13. Magafa, V., Stavropoulos, G., Zafiropoulos, T., Laussac, J., Hadjiliadis, N. *C. R. Acad.. Sci. Paris*. **1992**, *315*, 169-174.
14. Katono, Y., Inoue, Y., Chuju, R.. *Polymer Journal*. **1977**, *9*, 471-478.
15. Brubaker, G., Sakkab, N. *Inorg. Chem*. **1974**, *3*, 243-260.

16. Klemens, A., McMillin, D., Tsang, H., Peter-Hahn, J. *J. Am. Chem. Soc.* **1989**, *111*, 6398-6402; Sudmeier, J. and Perkins, T. *J. Am. Chem. Soc.* **1977**, *99*, 7732-7733; Libscomb, W., Reeke, G., Hartstuck, J., Quioco, F. Bethge, P. *Phil. Trans. Roy. Soc. London.* **1970**, *B257*, 177-214.
17. Ueyama, N., Kajiwara, A., Terakawa, T., Ueno, S., Nakamura, A. *Inorg. Chem.* **1985**, *24*, 4700-4704.
18. Mikulick, P., Riede, J., Schmidbaur, H. *Chem. Ber.* **1991**, *124*, 2743-2746.
19. (a) Utschig, L., Wright, J., Dieckmann, G., Pecoraro, V., O'Halloran, T. *Inorg. Chem.* **1995**, *34*, 2497-2498. (b) Utschig, L., Bryson, J., O'Halloran, T. *Science* **1995**, *268*, 380-385. (c) Blake, P., Lee, B., Summers, M., Park, J., Zhou, Z., Adams, M. *New J. Chem.* **1994**, *18*, 387-395.
20. Arena, G., Ipmellizzeri, G., Maccarrone, G., Pappalardo, G., Sciotto, D., Rizzarelli, E. *J. Chem. Soc. Perkin Trans. 2.* **1992**, 371-376.
21. Oku, J., Ito, N., Inoue, S. *Makromol. Chem.* **1982**, *183*, 579-586.
22. Abderhalden, E., Geidd, W. *Fermentforschung.* **1930**, *12*, 518.
23. Anderson, G., Zimmerman, J., Callahan, K. *J. Am. Chem. Soc.* **1967**, *89*, 5012-5017.
24. Paquette, L. *Encyclopedia of Reagents for Organic Synthesis.* **1995**, *3*, 1751-1753.
25. Brett, T., Alexander, J., Stezowski, J. *J. Chem. Soc., Perkin Trans. 2.* **2000**, 1105-1111.
26. Kojima, Y., Yamashita, T., Ishino, Y., Hirashima, T., Kirotsu, K. *Chem. Soc. Japan, Letters.* **1983**, 453-4.
27. Kojima, Y., Yamashita, T., Ishino, Y., Hirashima, T., Miwa, T. *Bull. Chem. Soc. Japan.* **1983**, *56*, 3481-3482.
28. Kojima, Y. *Chem. Soc. Japan, Letters.* **1981**, 61-62.
29. Kojima, Y., Hirotsu, K., Matsumoto, K. *Chem. Soc. Japan, Letters.* **1976**, 809-810.
30. (a) Coleman, J., *Methods Enzymol.* **1993**, *227*, 16-43. (b) Summers, M. *Coord. Chem. Rev.* **1988**, *86*, 43-134. (c) Ellis, P. *Science.* **1983**, *221*, 1141-1146.
31. Blake, P., Lee, B., Summers, M., Park, J., Zhou, Z., Adams, M. *New J. Chem.* **1994**, *18*, 387-395.

32. Utschig, L., Wright, J., Dieckmann, G., Pecoraro, V., O'Halloran, T. *Inorg. Chem.* **1995**, *34*, 2497-8.
33. Utschig, L., Baynard, T., O'Halloran, T. *Inorg. Chem.* **1997**, *36*, 2926-2927.
34. Marmorstein, R., Carey, M., Ptasne, M., Harrison, S., *Nature*. **1992**, *356*, 408-414.
(b) Church, W., Guss, J., Freeman, H. *J. Biol. Chem.* **1986**, *261*, 234-237.
35. Bebout, D., Stokes, S., Butcher, M. *Inorg. Chem.* **1999**, *38*, 1126-1133.

VITA

Christine M. Howard

The author was born in Plainfield, New Jersey, on December 1, 1978. She graduated from Broad Run High School in Ashburn, Virginia, in June of 1996, and The College of William and Mary in Williamsburg, Virginia, in May of 2000 with a B.S. degree in Chemistry.

After graduating with a M.A. degree in Chemistry, she hopes to continue her education and enter the medical field.